Parameterization retrieval of trace gas volume mixing ratios from airborne MAX-DOAS

Barbara Dix[1], Theodore K. Koenig,[1, 2] and Rainer Volkamer[1, 2]

[1]Institute for Chemistry and Biochemistry, University of Colorado, Boulder, CO, USA

5 [2]CIRES, University of Colorado, Boulder, CO, USA

Correspondence to: R. Volkamer (rainer.volkamer@colorado.edu)

Abstract. We present a parameterization retrieval of volume mixing ratios (VMR) from differential slant column density (dSCD) measurements by airborne multi-axis differential optical absorption spectroscopy (AMAX-DOAS). The method makes use of the fact that horizontally recorded limb

10 spectra (elevation angle 0°) are strongly sensitive to the atmospheric layer at instrument altitude. These limb spectra are analysed using reference spectra that largely cancel out column contributions from above and below the instrument, so that the resulting limb dSCDs, i.e., the column integrated concentration with respect to a reference spectrum, are almost exclusively sensitive to the atmospheric layers around instrument altitude. The conversion of limb dSCDs into VMRs is then realized by

15 calculating box-air mass factors (Box-AMFs) for a Rayleigh atmosphere and applying a scaling factor constrained by O_4 dSCDs to account for aerosol extinction. An iterative VMR retrieval scheme corrects for trace gas profile shape effects. Benefits of this method are 1) a fast conversion that only requires the computation of Box-AMFs in a Rayleigh atmosphere; 2) neither local aerosol extinction nor the slant column density in the DOAS reference (SCD_{ref}) need to be known; and 3) VMRs can be retrieved for

20 every measurement point along a flight track, in contrast to profile inversion techniques.

Sensitivity studies are performed for bromine monoxide (BrO), iodine monoxide (IO) and nitrogen dioxide (NO_2), using 1) simulated dSCD data for different trace gas and aerosol profiles; and 2) field measurements from the Tropical Ocean tRoposphere Exchange of Reactive halogen species and Oxygenated VOC (TORERO) field experiment. For simulated data in a Rayleigh atmosphere, the

25 agreement between the VMR from the parameterization method (VMR_{para}) and the true VMR (VMR_{true}) is excellent for all trace gases. Offsets, slopes and R^2 values for the linear fit of VMR_{para} over VMR_{true}

are as follows: BrO: (0.008 ±0.001) pptv, 0.988 ±0.001, 0.987; IO: (-0.0066 ±0.0001) pptv, 1.0021 ± 0.0003, 0.9979; NO_2: (-0.17 ±0.03) pptv, 1.0036 ±0.0001, 0.9997. The agreement for atmospheres with aerosol shows comparable R^2 values to the Rayleigh case, but slopes deviate a bit more from one: BrO: (0.093 ±0.002) pptv, 0.933 ±0.002, 0.907; IO: (0.0021 ±0.0004) pptv, 0.887 ± 0.001, 0.973; NO_2: (8.5

5 ±0.1) pptv, 0.8302 ±0.0006, 0.9923. VMR_{para} from field data are further compared with optimal estimation retrievals (VMR_{OE}). Least orthogonal distance fit of the data give the following equations: BrO_{para} = (0.1 ±0.2) pptv + (0.95 ±0.14) x BrO_{OE}; IO_{para} = (0.01 ±0.02) pptv + (1.00 ±0.12) x IO_{OE}; NO_{2para} = (1.7 ±8.0) pptv + (0.90 ±0.51) x NO_{2OE}. Overall, we conclude that the parameterization retrieval is accurate with an uncertainty of 20 % for IO, 30 % for BrO and NO_2, but not better than 0.05

10 pptv IO, 0.5 pptv BrO, and 10 pptv NO_2. The retrieval is applicable over a wide range of atmospheric conditions and measurement geometries, and not limited to the interpretation of vertical profile measurements in the remote troposphere.

1 Introduction

Airborne multi-axis differential optical absorption spectroscopy (AMAX-DOAS) measurements are

15 well suited to probe the vertical distribution of trace gases such as bromine monoxide (BrO), iodine monoxide (IO), nitrogen dioxide (NO_2), glyoxal (CHOCHO), formaldehyde (HCHO), nitrous acid (HONO) or the oxygen collision complex O_4 (Melamed et al., 2003; Wang et al., 2005, 2006; Heue et al., 2005, 2011, 2014; Bruns et al., 2006; Dix et al., 2009, 2013; Merlaud et al., 2011; Prados-Roman et al., 2011; Baidar et al., 2013a, 2013b; Oetjen et al., 2013; Baidar et al., 2015; Volkamer et al., 2015).

20 AMAX-DOAS collects scattered sun light along multiple lines of sight by changing the viewing direction of the light collecting telescope to different elevation angles (EA), here defined as the angle between horizon and line of sight. The selective combination of instrument and solar geometries maximizes sensitivity to different altitude layers in the atmosphere by enhancing the light paths through these layers. Generally MAX-DOAS measurements are most sensitive to absorbers at instrument

25 altitude when using low EAs, while the sensitivity to stratospheric trace gases depends mostly on solar zenith angle (Hönninger et al., 2004). Trace gas differential slant column densities (dSCD) are the primary product (level 1 data) when analysing scattered light spectra with the DOAS technique (Platt and Stutz, 2008). DSCDs quantify the integrated concentration along all light paths contributing to the

measured spectrum with respect to a reference spectrum, i.e. $dSCD = SCD - SCD_{ref}$, where SCD_{ref} is the slant column contained in the reference spectrum. In order to convert light path dependent dSCDs into a light path independent quantity, i.e., a vertical column density (VCD, the integrated concentration along a vertical column through the atmosphere), or a vertical concentration profile, the light paths

5   contributing to each dSCD measurement need to be known. Photon paths can be simulated by radiative transfer models (RTM). Since aerosol and clouds can strongly affect light path distributions, a typical method to retrieve VCDs or profile data from MAX-DOAS measurements is a two-step process: First, retrieval of the aerosol extinction profile, e.g., by utilizing information contained in measurements of O_4, (Wagner et al., 2004), which has an atmospheric profile that is well described by local temperature

10   and pressure (Thalman and Volkamer, 2013). Second, trace gas concentrations are retrieved through an inversion technique that applies RTM computed weighting functions for an atmosphere including the prior retrieved aerosol extinction. This approach is well suited for individual case studies, but it is time consuming and computationally intensive.

The widespread application of MAX-DOAS measurements from ground, ship, aircraft, balloon, and

15   satellite platforms and the accumulation of large data sets has led to recent developments that parameterize radiative transfer to interpret dSCD measurements (Sinreich et al., 2010, 2013; Irie et al., 2011; Schreier et al., 2016). Building on Sinreich et al. (2013), we present a parameterization retrieval of volume mixing ratios (VMRs) from AMAX-DOAS trace gas dSCDs. This study is organized as follows: Section 2 introduces the general principle of the retrieval. Section 3 describes a series of

20   sensitivity studies using simulated data, while Section 4 discusses errors, strengths and limitations of the method. The parameterization retrieval is then applied to TORERO field data in Sect. 5. Agreement with select optimal estimation results is evaluated and TORERO IO and BrO results are discussed. Section 6 summarizes results and concludes on strengths and limitations of the retrieval.

2 Parameterization retrieval

25   ### 2.1 General principle

The parameterization approach exploits the fact that spectra measured with EA 0° are highly sensitive to instrument altitude. An EA 0° spectrum is analysed relative to a suitable reference spectrum, e.g., a

zenith reference. As a result, trace gas contributions from atmospheric layers above and below the instrument are mostly cancelled out and the respective dSCD is representative of a range of altitudes near the instrument altitude. The sensitivity of such an EA 0° dSCD measurement is quantified by box-air mass factors (Box-AMFs) that are calculated for a Rayleigh atmosphere. Box-AMFs describe the

5 sensitivity of a measurement to the partial VCD of an atmospheric layer. For optically thin absorbers, such as discussed here, the calculation of Box-AMFs is independent of the trace gas profile. Figure 1 shows dBox-AMFs (dBox-AMF = Box-AMF - Box-AMF$_{ref}$) simulated at 477 nm for an instrument altitude of 5.25 km and a zenith reference from 7.75 km. The Box-AMFs are calculated on a vertical grid with a total number of N layers, where each layer n has a constant grid height, dh, of 0.5 km up to

10 18 km, and 1-2.5 km grid boxes above. The strong enhancement of dBox-AMFs at instrument altitude indicates the greatly enhanced sensitivity of AMAX-DOAS at instrument altitude. The altitude range with the largest dBox-AMFs is called the sensitive range, S (grey shading in Fig. 1). It is demarked by lower and upper boundary layers, n_L and n_U. The lower boundary n_L is set to 1 km below the instrument layer, n_{instr}, while n_U is set to the altitude layer before the difference between two consecutive dBox-

15 AMFs is smaller than 10 %, and no more than 3.5 km above n_{instr}. Typically this amounts to about 90 % of the sum over the dBox-AMF trace when measurement and reference spectrum are close in time.

The basis of the parameterization retrieval is to treat each EA 0° dSCD as a measurement of S, i.e. dSCD ≈ dSCD(S), and then retrieve the trace gas concentration for the layer n at instrument altitude, n_{instr}, (red shading in Fig. 1). To account for the effect of aerosol extinction on Box-AMFs in S, the

20 simultaneously measured O_4 dSCD is used as scaling factor. The concentration at instrument altitude, $c_{n_{instr}}$, is derived iteratively in molecules per cubic cm (molec/cm^3), with i iterations, using the following equation:

$$c_{n_{instr}}^i = (dSCD + dSCD_c^i) \cdot \frac{c(O_4)_{n_{instr}}}{O_4\ dSCD} \cdot f_c^i \qquad (1)$$

where dSCD is the trace gas dSCD measured at instrument altitude in molec/cm^2, dSCD$_c^i$ is a correction

25 term to account for remaining trace gas contributions from outside S (see Sect. 2.2 below), c(O_4)$_{ninstr}$ is the O_4 concentration in n_{instr} in molec^2/cm^6, and O_4 dSCD is the simultaneously measured O_4 slant

column in molec^2/cm^5. Since the equilibrium constant for O_4 is not well known, the O_4 concentration is scaled to the square of the oxygen concentration. Based on temperature and pressure profiles, the O_4 distribution can be calculated to an accuracy of better than 10^{-3} (Thalman and Volkamer, 2013). f_c^i is a unitless correction factor that accounts for differences in profile shape and absorption wavelength between O_4 and the trace gas of interest. It is defined as:

$$f_c^i = \frac{f_{O_4}}{f_{TG}^i \cdot f_{WL}}$$ (2)

The retrieval calculates f_c^i iteratively based on changes in f_{TG}^i according to:

$$f_{TG}^i = \frac{\sum_{n_L}^{n_U} c_n^i \cdot dBAMF_n}{c_{n_{instr}}^i \cdot \sum_{n_L}^{n_U} dBAMF_n}$$ (3)

where $dBAMF_n$ is the dBox-AMF value in layer n. The initial iteration, $i=0$, assumes that the trace gas concentration c_n^0 is constant inside S. Subsequent iterations calculate f_{TG}^i and f_c^i using prior iteration c_n^i values retrieved during aircraft ascent or descent. Concentration values between maximum aircraft altitude and n_U are interpolated using relative profile information from an atmospheric model. Convergence is typically achieved after the third iteration ($i=2$) (see Fig. S1.)

The factor f_{O_4} accounts for the O_4 profile shape in combination with the measured O_4 dSCD from Eq. (1). It is calculated as:

$$f_{O_4} = \frac{\sum_0^N c(O_4)_n \cdot dh \cdot dBAMF_n}{c(O_4)_{n_{instr}} \cdot \sum_{n_L}^{n_U} dh \cdot dBAMF_n}$$ (4)

All Box-AMFs are simulated for the wavelength of the trace gas of interest (see Table 1). The difference in absorption wavelength between the measured O_4 and trace gas dSCD is accounted for by f_{WL}:

$$f_{WL} = \frac{a_n(\lambda)}{O_4 \, dSCD} + b_n(\lambda) + c_n(\lambda) \cdot O_4 \, dSCD$$ (5)

where $a_n(\lambda)$, $b_n(\lambda)$, and $c_n(\lambda)$ are wavelength dependent 2nd order polynomial coefficients for each altitude layer n. The polynomial coefficients are derived by first simulating O_4 dSCDs for different aersosol extinction profiles at all O_4 and trace gas wavelengths, and then applying altitude dependent

fits to O_4 dSCDs at each trace gas wavelength plotted over O_4 dSCDs at the nearest O_4 wavelength. See Sect. 3.1.2 for further details.

The volume mixing ratio at instrument altitude, VMR_{ninstr}, is derived by dividing the final iteration c_{ninstr}^i derived with Eq. (1) by the air number density of n_{inst}. All VMRs in this study are expressed in pptv,

5   i.e., parts per trillion (1×10^{-12}) by volume.

Since more than half of the O_4 concentration profile is located below 4 km, the suitability of O_4 as scaling factor with increasing altitude needs to be assessed. Figure 2 investigates the altitude dependent sensitivity of O_4 measurements. Panel a) shows EA0° SCD and dSCD measurements simulated for a Rayleigh atmosphere for a solar zenith angle (SZA) range between 0° and 70°. The reference spectrum

10 to create dSCDs has a SZA of 25° and is from 14.75 km altitude, which is the maximum altitude for this study and representative of the range of altitudes covered during the TORERO project. Values above 15 km are included for reference, since some other research aircraft have the capability to access these higher altitudes. The comparatively strong O_4 absorption allows the significant detection of O_4 dSCDs of up to 20 km at 477 nm and up to 18 km at 360 nm, assuming a detection limit of 2×10^{41} molec^2/cm^5

15 and 5×10^{41} molec^2/cm^5 respectvely, which means that O_4 detection is not a limiting factor for the altitude range of this study. Moreover, Fig. 2b shows the fraction of the O_4 signal coming from outside the sensitive range S, for both SCDs and dSCDs. On average only 10 % of the dSCD signal originates from outside S, which makes the O_4 dSCDs very suitable for use as scaling factor. Increasing fractions below 5 km at 360 nm are due to stronger Rayleigh scattering, which decreases the vertical extent of S

20 and the magnitude of the dBox-AMF forward peak. Even though O_4 SCDs are not directly used for the parameterization retrieval, the increase of outside contributions to the total O_4 SCD with altitude are an indication of the increased error sensitivity of the O_4 dSCD towards inaccurate subtraction of outside contributions by the reference spectrum. We conclude that using measured O_4 dSCDs as an aerosol scaling factor is limited to altitudes below 15 km. For further discussion on the O_4 dSCD error see Sect.

25 4.

2.2 Correction of dSCD contributions from outside S

The accuracy of c_{ninstr} retrieved with Eq. (1) depends on the availability of a reference spectrum to cancel out dSCD contributions from above and below the sensitive range S. For example a difference in SZA between reference and measurement can lead to significant EA0° dBox-AMFs values outside S

5   and thus create significant dSCD contributions from outside S, particularly for absorbers with a large stratospheric VCD. The additive term $dSCD_c^i$ is included to account for tropospheric and stratospheric contributions from outside S:

$$dSCD_c^i = dSCD_{trop}^i + dSCD_{strat} \tag{6}$$

The tropospheric slant column correction, $dSCD_{trop}^i$ is defined as:

10    $$dSCD_{trop}^i = -dh \cdot \sum_{n_0}^{n_{max}} c_n^i \cdot dBAMF_n \qquad \text{for } i > 0 \text{ and } n \neq n_L \ldots n_U \tag{7}$$

$dSCD_{trop}^i$ is calculated from the surface to maximum aircraft altitude (layer n_{max}) for all n below n_L and above n_U using prior iteration c_n^i values retrieved during aircraft ascent or descent, which are also used in Eq. (4). For $i = 0$, c_n^0 is set to zero and hence $dSCD_{trop}^i$ is zero. Note that the distinction between tropospheric and stratospheric contributions is based on aircraft maximum altitude here, not on actual

15   tropopause height.

The stratospheric correction is calculated from layer n_{max} to N, i.e., the top of the atmosphere, and is applied to absorbers with a significant stratospheric VCD, here, BrO and NO_2. If n_{max} were not to cover most of the troposphere, the inclusion of $dSCD_{strat}$ also for tropospheric absorbers might become necessary. The stratospheric correction is based on upward looking EA 10° dSCD measurements at

20   n_{max}. We use EA 10° spectra instead of zenith spectra, because EA 10° measurements have a greater photon flux and therefore have a better signal to noise ratio, which is particularly helpful for measurements above 10 km aircraft altitude and below 400 nm. Further, the EA 10° geometry is more sensitive towards the atmosphere above n_{max} than a zenith spectrum. The stratospheric slant column correction term, $dSCD_{strat}$, is then defined as:

25    $$dSCD_{strat} = VCD(t_0)_{strat} \cdot AMF(t_0)_{ref_{strat}} - VCD(t)_{strat} \cdot AMF(t)_{ref_{strat}} - \Delta dSCD(t) \tag{8}$$

where $AMF(t_0)_{refstrat}$ is the air mass factor (AMF) of the zenith reference, recorded at time t_0, which was used to analyse both EA 0° and EA 10° dSCDs; $AMF(t)_{refstrat}$ is the air mass factor for a zenith reference at the same reference altitude, but calculated with the SZA at time t, i.e., the time of measurement; $VCD(t_0)_{strat}$ and $VCD(t)_{strat}$ are the stratospheric VCDs at the time of reference and measurement respectively. $\Delta dSCD(t)$ accounts for remaining stratospheric contributions from outside S at time t and is defined as:

$$\Delta dSCD(t) = dAMF(t, EA0°)_{above} \cdot VCD(t)_{strat} \cdot \frac{(AMF(t,EA10°)_{strat} - AMF(t,EA10°)_{in})}{AMF(t,EA10°)_{above} - AMF(t,EA10°)_{in}} \qquad (9)$$

where the subscript "in" refers to layers between n_{max} and n_U and "above" to layers (n_U +1) to N. AMFs and dAMFs are the sum over Box-AMFs/dBox-AMFs scaled by the trace gas profile. The profile information comes from an atmospheric model.

$VCD(t_0)_{strat}$ is derived by dividing the EA 10° dSCD at time t_0 by $dAMF(t_0, EA10°)_{strat}$. Contributions from layers below n_{max} to the EA 10° dSCD are assumed to be cancelled out by the reference. $VCD(t)_{strat}$ at the time of measurement is calculated as EA 10° dSCD(t) + SCD(t_0)$_{refstrat}$ divided by $AMF(t, EA10°)_{strat}$. Here, SCD and AMF are used instead of dSCD and dAMF to avoid increased uncertainties created by the division of two small numbers. The stratospheric amount contained in the reference, SCD(t_0)$_{refstrat}$, can easily be calculated from $VCD(t_0)_{strat}$. When reference and measurement are close in time, dSCD$_{strat}$ approaches $\Delta dSCD(t)$.

3 Application to synthetic data

In order to define filter criteria for conditions under which the parameterization retrieval is suitable for field data, a series of sensitivity studies were conducted, using synthetic data. The synthetic data set consists of BrO, IO, and NO$_2$ dSCDs simulated for different trace gas and aerosol extinction profiles (Fig. 3). Details on the setup are provided in the following Sect. 3.1. BrO and NO$_2$ are both gases for which a significant portion of the total VCD resides in the stratosphere. IO, CHOCHO and HCHO are mostly tropospheric absorbers, for which IO is discussed here as an example. The parameterization retrieval is first tested on trace gas dSCDs simulated for a Rayleigh atmosphere followed by a study on

how the VMR retrievals of the same trace gas profiles are affected by different aerosol extinction profiles.

3.1 Setup

3.1.1 Trace gas and aerosol profiles

5 Vertical trace gas profiles of BrO, IO and NO_2 as well as aerosol extinction profiles used to simulate dSCD data are shown in Fig. 3. There are three different profiles for each trace gas, named a, b, and c. The a-profiles peak strongly in the boundary layer and have a constant mixing ratio throughout the troposphere above. The NO_2 a-profile is selected to represent a polluted boundary layer. All b-profiles exhibit an elevated layer. The IO b-profile is based on TORERO measurements near the coast of

10 Antofagasta, Chile, where an IO layer around 2 km altitude was observed (see also Fig. 7). The NO_2 b-profile overlaps with the aerosol extinction layer of extinction profile 3, simulating an elevated pollution layer. BrO and IO c-profiles are TORERO campaign averages for the tropics. The NO_2 c-profile is a case study from TORERO research flight (RF) 12 as published in Volkamer et al. (2015). Tropospheric VCDs from the surface to 18 km for a-, b-, and c-profiles are 1.4×10^{13} molec cm^{-2}, 2.4×10^{13} molec

15 cm^{-2}, and 1.7×10^{13} molec cm^{-2} for BrO, 5.0×10^{12} molec cm^{-2}, 8.6×10^{12} molec cm^{-2}, and 3.4×10^{12} molec cm^{-2} for IO, and 42.5×10^{14} molec cm^{-2}, 8.0×10^{14} molec cm^{-2}, and 2.7×10^{14} molec cm^{-2} for NO_2, respectively. Stratospheric profiles for BrO and NO_2 are similar to conditions found in the TORERO study area with $VCD_{strat} = 1.1 \times 10^{13}$ molec cm^{-2} and 1.3×10^{15} molec cm^{-2} for BrO and NO_2 respectively (see Fig. S2 for profile shape). IO profile concentrations are 0 above 18 km. The aerosol

20 extinction profiles vary in shape, absolute values and composition. Profiles 1 through 3 (Fig. 2) are assumed to represent a clean marine (1), a polluted urban (2) and a semi polluted (3) environment. The latter consists of marine aerosols in the boundary layer and an urban pollution layer aloft. Details on the representation of aerosol in the RTM are given in the following Section and Table 1.

3.1.2 Radiative transfer modelling

25 All Box-AMFs used in this study are calculated with McArtim (Deutschmann et al., 2011), which is a fully spherical Monte Carlo radiative transfer model. Table 1 provides a summary of RTM settings that

were used to compute Box-AMFs for the sensitivity studies. The SZA is varied between 0° and 70°, while the solar relative azimuth angle (SRAA) is kept constant at 90°. All model calculations are performed on a 0.5 km vertical grid, which is representative of the vertical resolution of our TORERO AMAX-DOAS measurements. EA 0° measurements are simulated for 0.1 km and from 0.25 to 14.75

5   km in 0.5 km steps. For zenith spectra, the reference altitude, h_{ref}, is varied between 0.1 km and 12.25 km (see Table 1). Above 12.5 km, the zenith sky is considered too dark to obtain high quality spectra. EA 10° reference spectra are simulated for altitudes between 11.25 km and 14.75 km (see Table 1). Reference selection is further discussed in Sect. 3.1.3. The model wavelengths for which Box-AMFs are calculated are selected to match the centre wavelength of individual trace gas DOAS fitting windows

10   (Volkamer et al., 2015; Wang et al., 2015), i.e., 350 nm for BrO, 428 nm for IO, 447 nm for NO_2, and 360 nm and 477 nm for O_4. The model atmosphere is set up to represent conditions over a tropical ocean as found during TORERO. It includes profiles of ozone (VCD = 7.0 x 10^{18} molec cm^{-2} / 260.2 DU), H_2O (VCD = 1.79 x 10^{23} molec cm^{-2}), NO_2 (VCD = 2.76 x 10^{16} molec cm^{-2}) and O_4 (VCD = 1.39 x 10^{43} molec^2 cm^{-5}). The O_4 profile is corrected for oxygen displacement by water vapor, because the

15   very high water mixing ratios found in the tropical marine boundary layer can decrease collocated O_4 concentrations by up to 5 % (Thalman and Volkamer, 2013; Spinei et al., 2015). Surface temperature, pressure and water mixing ratio are 300.2° K, 1010.5 mbar and 3.1 % respectively. Aerosols are included using extinction profiles (Fig. 2), single scattering albedo (SSA) and the g-parameter as representation for the aerosol phase function (Henyey and Greenstein, 1941). Values for SSA and g-

20   parameter are chosen based on Fig. 1 and Table 1 in Dubovik et al. (2002). To simulate trace gas and O_4 SCDs at other wavelengths, aerosol extinction profiles are scaled from 477 nm assuming an Ångström exponent of 1. DSCDs are created using references as described below (Sect. 3.1.3). In order to get the wavelength and altitude dependent fit coefficients that define f_{WL}, (Eq. (5)), O_4 dSCDs simulated for all extinction profiles are separated by altitude layers n. For each n, respective O_4 dSCDs at 447 nm and

25   428 nm are each plotted over O_4 dSCDs at 477 nm and fitted with a 2nd order polynomial. The same is done for O_4 dSCDs at 350 nm, but plotted over O_4 dSCDs at 360 nm. The resulting wavelength and altitude dependent fit parameter are used as a lookup table and applied in Eq. (5) during the VMR retrieval to interpolate the measured O_4 dSCDs from Eq. (1). The same process of is applied to

interpolate Rayleigh Box-AMFs from 477 nm to 447 nm and 428 nm, and from 360 nm to 350 nm, in order to save RTM computation time. E.g. for a near real-time application of the parameterization retrieval during a field project, a significant amount of computation time can be saved when for each (new) research flight, Box-AMFs along the flight track only need to be calculated at two wavelengths,

5   instead of at all trace gas wavelengths.

3.1.3 Reference spectra

For a detailed discussion on suitable references for BrO, IO and NO_2 see Volkamer et al. (2015). For our sensitivity studies, BrO and NO_2 are analysed with a zenith reference (EA 90°). Since the sky becomes increasingly dark with altitude, upward looking EA 10° spectra from aircraft maximum

10   altitude are a light strong alternative for absorbers without significant stratospheric VCDs. O_4 and IO are therefore analysed with high altitude EA 10° references. A further advantage of EA 10° references is that in the presence of aerosols EA 10° Box-AMFs from high altitude spectra resemble EA0° Box-AMFs outside S more closely than those of zenith references, thus cancelling out distributions from outside S more accurately (Volkamer et al., 2015). Altitudes for both zenith and EA 10° references are

15   listed in Table 1. For IO, trace gas and O_4 references are identical. When retrieving BrO and NO_2, O_4 is analysed with an EA 10° reference from aircraft maximum altitude, here 14.75 km. Trace gas and O_4 references have the same SZA.

3.2 Sensitivity studies

SCDs were simulated for all trace gas and aerosol extinction profiles shown in Fig. 3 and for settings

20   summarized in Table 1. Parameters of interest that are varied are SZA, ΔSZA, i.e., the SZA difference between EA 0° and reference measurement, and the reference altitude h_{ref}. Trace gas dSCDs were created by permuting through every reference for each combination of trace gas and aerosol profiles, for a total of 2940 different full profile case studies. For the VMR retrieval only dSCDs larger than 1.5 x 10^{13} molec cm^{-2} for BrO, larger than 2 x 10^{12} molec cm^{-2} for IO, and larger than 2 x 10^{14} molec cm^{-2} for

25   NO_2 are considered as significant, and smaller dSCDs were filtered. These limits are based on typical fit uncertainties for the University of Colorado (CU) AMAX-DOAS instrument. For trace gases with

stratospheric VCDs, the maximum SZA is limited to 60°, creating a total of 2160 different full profile case studies for BrO and NO_2. IO dSCD data above h_{ref} are removed for test cases where h_{ref} is below aircraft maximum altitude. Further filtering is based on the results of the sensitivity studies and discussed in Sect. 3.2.2.

3.2.1 VMR$_{para}$ in a Rayleigh atmosphere

Figure 4 presents a summary of VMR retrieval results from trace gas dSCDs simulated for a Rayleigh atmosphere for 735 IO and 540 BrO and NO_2 profile case studies and for $i=2$ (see Fig. S3 for a comparison of $i=0$ and $i=2$). Results are displayed separately for each trace gas and profile shape. All retrieved VMR$_{para}$ are binned by EA 0° instrument altitude (see Table 1). For each altitude, the average and standard deviation of VMR$_{para}$ is calculated and plotted in the individual left panels of Fig. 4 together with the original trace gas profile as reference. The green shading indicates ±0.5 pptv for BrO, ±0.05 pptv for IO and ±10 pptv for NO_2. To get further information on the distribution of retrieved VMRs, ratios of VMR$_{para}$ over true VMR, VMR$_{true}$, are calculated. These ratios are separated by trace gas and profile shape and plotted as vertically resolved whiskers in the individual right panels of Fig. 4. Whiskers denote 5, 25, 75 and 95 percentiles. A ratio of 1 means VMR$_{para}$ is retrieved without error. Grey shaded areas indicate 15 % and 30 % error respectively. Dark green dashed lines show the equivalent of ±0.5 pptv, 0.05 pptv and 10 pptv for BrO, IO, and NO_2, respectively, calculated by adding or subtracting the respective amount from the true profile before division by the true profile. For select cases, scaled equivalents are included, based on a ±(0.5 pptv x 0.1) scaling for BrO and ±(10 pptv x 0.1) for NO_2. The agreement between retrieved and true VMRs is excellent for all trace gases and profile shapes. Even 5 and 95 percentile whiskers fall within the 30 % error margin or better. These results demonstrate the accuracy of the stratospheric correction for BrO and NO_2. For BrO and NO_2 c-profiles the true mixing ratio falls within 0.5 pptv and 10 pptv respectively. The comparison of the 5 and 95 percentiles indicates a slight low bias of the retrieved VMRs for both BrO and NO_2 across all profile shapes. This bias is primarily caused by negative ΔSZAs, i.e. the SZA of the reference is higher than the SZA of the measurement. The impact of ΔSZA < 0° can be seen in Fig. S3, which shows select VMR$_{para}$ data color coded by SZA, ΔSZA and h_{ref}. SZA here and in the following always refers to the SZA of the

measurement spectrum, not the reference. For $i=0$ the general trend in the retrieved VMRs is that the relative deviation from the true profile increases with increasing SZA. For ΔSZA < 0, VMR_{para} values underestimate the true profile. This is similarly true for reference spectra recorded at low altitudes, e.g. 0.1 km for zenith spectra (BrO and NO_2) and 11.25 km for EA° 10 spectra (IO). The iterative

5 corrections applied during the VMR retrieval significantly improve final results, especially for BrO. The retrieval of IO VMRs is very robust and shows no strong sensitivities to variations in SZA, ΔSZA or h_{ref}, regardless of iteration status. The final VMR_{para} results for $i=2$ are within ±0.5 pptv for BrO, ±0.05 pptv for IO, and ±10 pptv for NO_2. While the errors created by a changing SZA and low h_{ref} are essentially eliminated by the iterative corrections, a low bias caused by ΔSZA < 0° remains for BrO and

10 NO_2. E.g., the VMR ratio of the BrO c-profile at 11.25 km altitude with ΔSZA = -40° and h_{ref} = 0.1 km is 0.87, while the ratio at the same altitude with ΔSZA = 15° and h_{ref} = 0.1 km is 1.01. Corresponding ratio values for the NO_2 b-profile are 0.85 and 0.99. For all 540 Rayleigh profile cases, 100 % of BrO VMR_{para} data is retrieved within ±0.5 pptv of the true profile. Where the true profile falls below 0.5 pptv, 100 % is retrieved within 0.5 pptv. For NO_2 96.7 % of VMR_{para} data are reproduced within ±10

15 pptv and 100 % of VMRs below 10 pptv are retrieved within the limit. Where VMR_{para} is outside ±10 pptv of VMR_{true}, 85.8 % are retrieved within 30 % of $VMR_{true.}$ For all 735 IO profile cases, 99.4 % of VMR_{para} data is retrieved within ± 0.05 pptv. A summary of these results is included in Table 2 below. Based on these results, we define 0.5 pptv, 0.05 pptv, and 10 pptv for BrO, IO, and NO_2 respectively as 1) suitable detection limits, and 2) in combination with a 20 % (IO) and 30 % (BrO) error suitable error

20 bounds for the parameterization method in a Rayleigh atmosphere.

3.2.2 VMR_{para} in aerosol atmospheres

The presence of aerosol in the atmosphere changes Box-AMFs; this is accounted for in the parameterization retrieval by using a measured O_4 dSCD in Eq. (1) to scale Rayleigh modelled Box-AMFs. In comparison to results from a Rayleigh atmosphere, the quality of retrieved VMRs in

25 atmospheres with aerosol shows a stronger and more complex dependency on SZA, ΔSZA and h_{ref}. Therefore Fig. 5 presents results for select case studies, to highlight these specific dependencies. Summary figures for individual extinction profiles in the style of Fig. 4 are provided in the SI (Figs. S4-

S6) and discussed in Sect. 4.3. Figure 5 shows VMR_{para} plotted over VMR_{true} for select SZA, ΔSZA and h_{ref}. BrO and IO VMR_{para} are averaged over all trace gas and aerosol profiles. NO_2 results are averaged over NO_2 b- and c- profiles (Fig. 3) and all aerosol profiles. Averages of the NO_2 a-profile are shown in Fig. S7. A total of eight case studies are displayed in panels a) through h). Panel columns

5   alternate between low and high SZA (25° and 60°). Rows highlight the dependency on ΔSZA for ΔSZA = 0°, 35°, and -15°, in combination with a variation of h_{ref}. Panels a), b), e), and f) show results with h_{ref} = 4.25 km for BrO and NO_2, and h_{ref} = 14.75 km for IO, which are considered to be optimal references for our case studies. Panels c) and d) display the effect of using a zenith reference from 0.1 km, while panels g) and h) show results for a high zenith reference. For a direct comparison, IO data in panels c),

10   d), g) and h) is also analysed with zenith references. VMR_{para} data for each panel summarizes over nine profile cases for BrO and IO, and over six cases for NO_2. Whisker plots show 5, 25, 75 and 95 percentiles for binned VMR data. VMRs for BrO are binned in 0.5 pptv intervals and for IO in 0.25 pptv intervals. NO_2 bins are defined as follows: 20 pptv intervals from 0-80 pptv, then 80 pptv-150 pptv, 150 pptv-400 pptv and 400 pptv-1300 pptv. Linear fits to VMR_{para} and respective fit parameters,

15   "s" for slope, "o" for offset, are included in each panel. Grey shadings indicate 15 % and 30 % error respectively.

Effect of SZA: VMR retrievals for BrO and NO_2 show a stronger dependency on SZA than those of IO, which can be expected for trace gases with a significant stratospheric VCD. For SZA = 25° and the optimal h_{ref}, i.e., panels a) and e), BrO and NO_2 correlation slopes are on average 0.95 ±0.01 and 0.905

20   ±0.015. Offsets are all below the respective detection limits of 0.5 pptv for BrO and 10 pptv for NO_2 and R^2 values are 0.96 (a))/0.97 (e)) for BrO and 0.94 a) and e) for NO_2. Results for SZA = 25° and h_{ref} = 12.25 km (panel g)) are comparable for both BrO and NO_2. Higher SZAs increase the stratospheric contribution to the measured dSCDs, which creates a stronger sensitivity to errors in the stratospheric correction. BrO and NO_2 VMR_{para} for SZA = 60° with h_{ref} = 4.25 km and 12.25 km (panels b), f), and

25   h)) show somewhat lower correlation slopes that are on average 0.89 ±0.02 for BrO and 0.87 ±0.02 for NO_2, but offsets remain below respective detection limits and average R^2 values are still high with 0.96 ±0.01 for BrO and 0.93 ±0.01 for NO_2. When looking at the NO_2 a-profile only (Fig. S7), then the linear fits are strongly driven by the very high boundary layer VMRs, which is why the NO_2 data set is

separated by profile shape here. For the NO_2 a-profile the SZA dependence is much more pronounced. For optimal and high references, correlation slopes are around 0.91 for SZA = 25° and around 0.81 for SZA = 60°. In contrast, when using a high altitude reference spectrum for IO, panels a), b), e) through h), correlation slopes are within ±2 percentage points and corresponding offsets are 0.003-0.029 pptv,

5 which is well below the 0.05 pptv detection limit. R^2 values are between 0.970 and 0.990.

Effect of ΔSZA and h_{ref}: The impact of ΔSZA and h_{ref} depends on the combination of both quantities. When using either the optimal or high reference altitude, i.e. panels a), b), e) through h), the VMR results for all trace gases are dominated by the SZA effect, as discussed above. Varying ΔSZA between 0°, 35°, and -15° for a constant SZA, i.e. comparing panels a), e), g) and panels b), f), h), leads to

10 differences in correlation slopes that are within ±0.02. Interestingly, a ΔSZA of zero does not always provide the best results, the reason being that a larger difference in SZA between reference and measurements can actually increase the accuracy of the correction term f_c (Eq. (1)). Overall, the combination of ΔSZA = -15° or 35° with a zenith reference from the boundary layer (0.1 km altitude) yields the largest deviations of VMR_{para} from VMR_{true} for all trace gases. E.g., for BrO, panel c) the

15 correlation slope drops to 0.89 with R^2 = 0.84; for IO c) the slope is 0.845 with an R^2 of 0.981, and NO_2 in panel c) has a slope of 0.84 and R^2 = 0.92. The NO_2 a-profile shows comparable behaviour in panel d), with a slope of 0.77 (Fig. S7). Overall the observed trends are significantly reflected in correlation slopes and R^2 values, while offsets are typically very small and well below 50 % of the individual trace gas detection limit. Slopes for optimal and high reference spectra indicate that on average VMR_{para} are

20 retrieved within 10 to 15 % of VMR_{true} with tight correlations, i.e., R^2 values of 0.92 and better. Based on the combined effect of low h_{ref} and ΔSZA < 0° an additional filter for the parameterization retrieval is introduced: VMR retrieval of trace gases with stratospheric VCDs are limited to ΔSZA > -25° for h_{ref} < 2 km. Following the error discussion, results of the full set of sensitivity studies are discussed in Sect. 4.3.

4 Error analysis and discussion

4.1 Retrieval error

The underlying assumption of Eq. (1) is that dSCD ≈ dSCD(S), i.e., that the EA 0° dSCD measurement quantifies the trace gas slant column in S (see Sect. 2.1 and Fig. 1). How well this assumption holds true

5   depends on the choice of reference spectrum and the accuracy of the iterative correction term $dSCD_c^i$ introduced in Eqs. (6) through (9). The same assumption underlies the measured O_4 dSCDs. Further error sources are insufficient correction of the O_4 and trace gas profile shapes based on Eqs. (3) and (4), and errors caused by the wavelength interpolation of measured O_4 dSCDs based on Eq. (5). The synthetic data set allows the quantification of individual error sources, and the overall error. The

10   following error terms are being analysed here: the error of $dSCD_c^i$, the errors of f_{TG}^i, f_{O4}, and f_{WL}. The magnitude of each error is defined as the ratio of calculated value over true value, which returns 1 when the error is 0. The $dSCD_c^i$ error ratio, $\Delta dSCD_c^i$, is defined as (dSCD - $dSCD_c^i$) divided by dSCD(S). For the f_{TG} error ratio, Δf_{TG}^i, the value of f_{TG}^i calculated with Eq. (3) is divided by the true f_{TG}, i.e. using Eq. (3) and replacing c_n^i with the true trace gas concentration. The f_{O4} error ratio, Δf_{O4}, summarizes the error

15   caused by applying O_4 dSCDs as scaling factor for Rayleigh modeled Box-AMFs. Based on Eq. (1), it is defined as:

$$\Delta f_{O_4} = \frac{c(O_4)n_{instr}}{O_4\ dSCD} \cdot f_{O_4} \cdot \sum_{n_L}^{n_U} dh \cdot dBAMF(aer)_n \qquad (10)$$

where dBAMF(aer) are the Box-AMFs simulated for the specific aerosol profile. The f_{WL} error ratio, Δf_{WL}, quantifies the ratio of wavelength shifted O_4 dSCDs using Eq. (5) over O_4 dSCDs directly

20   simulated at the respective trace gas wavelength. Note that these error ratios are not random errors, but express a systematic deviation from the true value, which can be calculated for each retrieved VMR data point. The total error ratio, $\Delta total$, is defined as the deviation of the calculated trace gas concentration from the true trace gas concentration and is thus identical to VMR_{para} over VMR_{true}. It can be directly calculated from the above introduced error ratios using Eq. (1) as follows:

25   $$\frac{VMR_{para}}{VMR_{true}} = \Delta total = \Delta dSCD_c^i \cdot \frac{\Delta f_{O_4}}{\Delta f_{TG}^i \cdot \Delta f_{WL}} \qquad (11)$$

Note that this notation is chosen because it explicitly accounts for the fact that individual component errors can compensate each other. All error calculations are performed for $i = 2$. For Rayleigh cases both Δf_{O4} and Δf_{WL} are 1.

Figure 6 shows examples of error ratios plotted over altitude and separated by trace gas and aerosol extinction profiles with SZA = 25°, ΔSZA = 25°, and h_{ref} = 4.25 km for BrO and NO$_2$, and h_{ref} = 14.75 km for IO. Results are shown for BrO c-, IO b- and NO$_2$ b-profiles. Error ratios for all trace gas profiles are included in the SI (Figs. S8-S10). In Fig. 6, Δf_{TG}^{i} and Δf_{WL} are plotted inverse in accordance with the fact that they enter the denominator in Eq. (11).

$\Delta \mathbf{dSCD_c^i}$: Error ratios from $dSCD_c^i$ are the dominating error source in a Rayleigh atmosphere and remain a comparatively large error source for atmospheres with aerosols for all trace gases. This is a direct reflection of how well the assumption $dSCD \approx dSCD(S)$ holds true. At the selected solar and measurement geometry conditions, $dSCD_{trop}^i$ and $dSCD_{strat}$ are comparable for both the BrO c-profile and the NO$_2$ b-profile, with ~1 x 10^{12} molec/cm^2 for BrO and ~2 x 10^{14} molec/cm^2, which means that the combined tropospheric and stratospheric $dSCD_c^i$ correction is not dominated by either part of the profile. Stronger deviations are correlated with the absolute trace gas concentration and higher aerosol extinction. E.g. for the BrO c-profile in the boundary layer, $\Delta dSCD_c^i$ ranges between 1.5 and 2.7. Here the true profile is < 0.25 pptv, which means that the signal from inside S contributing to the EA 0° dSCD measurements is very small. The dashed lines in Fig. 6 show the equivalent of ±0.5 pptv BrO or the scaled equivalent of ±0.05 pptv as reference. Δtotal for all cases is well below the detection limit of ±0.5 pptv. However, the steep increase in deviations for all error ratios for the BrO c-profile below 4 km indicates that the accuracy of VMR$_{para}$ declines with decreasing dSCDs, and that using a detection limit is justified. A strong $\Delta dSCD_c^i$ deviation from 1 caused by the elevated aerosol layer of aerosol 3 (Fig. 3) is seen for IO and BrO. Here dSCDs are overcorrected, but this error is partially compensated by too low f_{O4}. Interestingly, $\Delta dSCD_c^i$ is smaller for the NO$_2$ b-profile, where the NO$_2$ profile itself has an elevated layer (Fig. 3).

Δf_{TG}^i: f_{TG}^i corrects for trace gas gradients within S. Hence deviations from 1 of Δf_{TG}^i are directly related to the trace gas profile shape. In a Rayleigh and sub-Rayleigh atmosphere (see Fig. 3) Δf_{TG}^i is on average around ±2 % and deviates only significantly from 1 where the VMR$_{true}$ profile has strong concentration gradients, e.g. around the IO layer between 2 and 3 km in the IO b-profile, around 7 km for the NO$_2$ b-profile, or around 2 km for all trace gas a-profiles (Figs. S8-10). The magnitude of the deviation depends on the aerosol extinction. For example, the peak in Δf_{TG}^i at 1.75 km in the IO b-profile changes from 1.12 to 1.27 between aerosol 1 and 2, where both extinction profiles have the same shape, but where aerosol 2 has a higher extinction (0.11 vs 0.02 km^{-1} at 1.75 km altitude). This is similarly true for the NO$_2$ a-profile (Fig. S10) at 0.1 km, where Δf_{TG}^i increases from 1.24 to 1.44 between aerosol 1 and 2 (Extinctions at 0.1 km are (0.188 vs 0.037 km^{-1}). The overlap of trace gas and aerosol extinction gradients as well as higher absolute extinction increases Δf_{TG}^i deviations from 1, which is typically the case for trace gas and aerosol profiles that represent polluted environments (Sect. 3.1).

Δf_{O4}: The f_{O4} error ratio generally follows the shape and magnitude of the extinction profile as can be expected. For NO$_2$ at 447 nm and IO at 428 nm, f_{O4} tends to overestimate the extinction in the boundary layer ($\Delta f_{O4} > 1$) and slightly underestimate the extinction in the free troposphere ($\Delta f_{O4} < 1$), where the aerosol extinction is sub-Rayleigh. For BrO, the effect is reversed in the boundary layer, and not significant in the troposphere. This result is caused by the differences in the wavelength dependency of Rayleigh and aerosol extinction. Box-AMFs scale with light path length. In the presence of aerosol, the total extinction is determined by Rayleigh and aerosol extinction. Since Rayleigh extinction scales with λ^{-4} and the aerosol extinction in our sensivity study scales with λ^{-1}, the (strong) aerosol extinction in the boundary at 447 and 428 nm has a comparatively stronger effect at wavelengths above 400 nm than at 350 nm where BrO is measured. The trend to underestimate extinction in the troposphere above 400 nm is caused by multiple scattering. While the presence of aerosol typically decreases the light path length at instrument altitude, and hence the Box-AMFs within S, increased scattering in aerosol layers below or above instrument altitude can lead to increased contributions from outside S to the measured O$_4$ dSCD. Thus the measured O$_4$ dSCD leads to the underestimation of the real extinction. This effect is amplified for the aerosol layer around 7 km of aerosol profile 3. Enhanced photon back scatter from the

boundary layer and the elevated aerosol layer increases the outside contributions to the O_4 dSCD measurements inside the layer further, which leads to Δf_{O4} values as low as 0.59 at 447 nm (NO_2), 0.58 at 428 nm (IO) and 0.75 at 350 nm (BrO). Interestingly, $\Delta dSCD_c^i$ inside the elevated aerosol layer is overestimated at all wavelengths, with a compensating effect on Δtotal.

5   Δf_{WL}**:** The error created by the wavelength interpolation of measured O_4 dSCDs is comparatively small. It increases with larger wavelength shifts, e.g. for IO, where O_4 dSCDs are shifted from 477 nm to 428 nm. The f_{WL} error ratio shows no significant altitude dependence, and is typically smaller than 5 %. The largest Δf_{WL} deviation from 1 is found at 7.25 km altitude for IO and aerosol 3, inside the elevated aerosol layer, with $\Delta f_{WL} = 0.86$. This larger deviation is caused by defining the polynomial coefficients

10   used in Eq. (5) as average over all extinction profiles. The reduction of EA 0° O_4 dSCDs at different wavelengths is not a linear function of extinction, and interpolation parameters at the altitude of the elevated aerosol layer are biased low by averaging O_4 dSCDs from aerosol profile 3 with O_4 dSCDs simulated for the sub-Rayleigh extinction of aerosol 1 and 2 at the same altitude. If the polynomial coefficients were generated using only aerosol profile 3, the same Δf_{WL} would increases to 0.92.

15   Notably, the elevated pollution layer is a unique case, and affects only a small number of IO and NO_2 VMR_{para} data within a 1.5 km altitude range (see also discussion in Sect. 4.3.1).

4.2 Other error sources

Other errors affecting the accuracy of VMR_{para} are RTM errors, and uncertainties in the atmospheric model profiles used to interpolate retrieved trace gas profiles above aircraft maximum altitude. The

20   RTM error encompasses the statistical error of simulating individual photon paths used to calculate the Box-AMFs, and the error created by wavelength shifting Box-AMFs (see Section 3.1.2). McArtim is initialized with 10^5 photons, which reduces the statistical error to below 0.5 % (see also Spinei et al., 2015). Table S1 gives fit coefficients of linear fits to shifted Box-AMF data over original data. Slopes are 0.999 with a 1-2 x 10^{-4} error and offsets are <= 0.003. Atmospheric model profiles are used to

25   interpolate trace gas profiles above aircraft maximum altitude and calculate stratospheric AMFs. Here, only the relative profile shape is important, since absolute VCD values are cancelled out during the

AMF calculation. Stratospheric profile shapes of BrO and NO_2 are well constrained by models, therefore the error based on profile shape is assumed to be very small and accounted for by the error bounds.

4.3 Summary and overall error

5 The sensitivity studies in a Rayleigh atmosphere have shown that the parameterization retrieval works very well across a wide range of measurement geometries. VMR retrievals in aerosol atmospheres are more sensitive to SZA and choice of reference spectrum. In Figs. S4-S6 VMR_{para} results for aerosol atmospheres are displayed using the style introduced in Fig. 4, i.e. left panels show mean and standard deviation of VMR_{para} and right panels show altitude resolved whisker plots of the ratio of VMR_{para} over

10 VMR_{true}. Note that in contrast to Fig. 5 the additional ΔSZA filter is applied here, where for BrO and NO_2 the VMR retrieval is limited to $\Delta SZA > -25°$ when $h_{ref} < 2$ km. Compared to a Rayleigh atmosphere the VMR_{para} distribution around the mean has a larger spread. Where the aerosol extinction is sub-Rayleigh (see Fig. 3), the mean stays close to 1 for BrO and NO_2. The effect of SZA, ΔSZA and h_{ref} discussed above is captured in the whisker percentiles. For IO the mean tends to deviate from 1

15 between 2 and 10 km, which is the effect of $\Delta dSCD_c^i$ that is intensified by Δf_{WL} and Δf_{O4} for atmospheres with aerosol as shown in Fig. 6. However, most VMR_{para} data is still retrieved within error bounds. Table 2 summarizes the mean and 1 sigma standard deviation of the ratio VMR_{para} over $VMR_{true,}$ for each trace gas separated by atmospheres. The column "within error" states the fraction of VMR_{para} that is retrieved either within the VMR detection limit, or within 30 % for BrO and NO_2 and 20

20 % for IO. The distinction in percentage is based on the stronger sensitivity to SZA, ΔSZA and h_{ref} for trace gases with stratospheric VCD. After filtering all VMR_{para} data is retrieved on average within 10 % of the error bounds or better.

Field data: When applying the parameterization retrieval to dSCD data from the TORERO measurements, dSCDs have associated measurement errors. To test the effect of dSCD errors, VMRs

25 for all trace gas and aerosol profiles were retrieved, adding or subtracting 1.5×10^{13} molec cm^{-2} for BrO, 2×10^{12} molec cm^{-2} for IO and for 2×10^{14} molec cm^{-2} for NO_2. The impact on VMR_{para} was assessed by adding the error caused by the measurement uncertainty and the parameterization error in

quadrature. On average 92.9 % of resulting VMR_{para} data are still retrieved within the above defined error bounds. The fit errors for O_4 dSCDs are typically well below 5 %, with absolute values $< 5 \times 10^{41}$ $molec^2/cm^5$ at 477 m, and $< 1 \times 10^{42}$ $molec^2/cm^5$ at 360 nm, and are accounted for by the error bounds. To avoid uncertainties created by fit errors, measured O_4 dSCDs are set equal to Rayleigh modeled

5   dSCDs when their absolute difference is smaller 5×10^{41} $molec^2/cm^5$ at 477 m, and smaller 1×10^{42} $molec^2/cm^5$ at 360 nm. The uncertainty in determining O_4 SCD_{ref} for the absolute scaling of measured O_4 dSCDs is essentially cancelled out by using dSCDs and considered negligible.

We conclude that 30 % uncertainty for gases with stratospheric VCD contributions, and 20 % for tropospheric absorbers, but no better than 0.5 pptv BrO, 10 pptv NO_2 and 0.05 pptv IO are suitable error

10   bounds for the parameterization retrieval across different trace gas and aerosol profiles. Errors and sensitivities that arise from strongly changing trace gas VCDs and atmospheric conditions when flying at level altitude will be discussed elsewhere.

4.3.1 Outliers

Some VMR_{para} data retrieved outside error bounds show significant and systematic deviations from

15   VMR_{true}. Examples of such outliers in Fig. 5 are in BrO panel b) the VMR_{para} points that deviate by about 0.6 pptv from VMR_{true}, IO panel b) deviations of 0.12 pptv from a true VMR of 0.3 pptv, and for NO_2 deviations of around 50 pptv for true values around 100 pptv across all panels. These outliers are not captured by data filtering. This is for example the case for the IO b-profile and aerosol profile 1 (Fig. S4), for BrO and NO_2 a-profiles and aerosol 2 (Fig. S5), or for IO and NO_2 b-profiles and aerosol

20   profile 3 (Fig. S6). When looking at the trace gas profile shapes of the individual left panels in Figs. S4-S6, it becomes apparent that strong gradients in the trace gas profile can shift the retrieved means significantly away from 1, with partial or full whiskers exceeding the error bounds. In a Rayleigh atmosphere, similar outliers are seen for $i = 0$, but the iterative corrections bring final VMR_{para} data well within error bounds (Sect. 3.2.1 and Fig. S3). In the presence of aerosols the iterative corrections fail

25   when trace gas and aerosol extinction gradients overlap, or where extinction is high, like in the lofted pollution layer of aerosol profile 3. These are highly localized effects, but need to be kept in mind when

using the parameterization retrieval in areas with strong trace gas and extinction gradients. Under those conditions, optimal estimation retrievals are preferred.

4.3.2 Impact of SCD_{ref}

The selection of a suitable reference spectrum is crucial to best fulfilling the approximation dSCD ≈

5   dSCD(S), which is applicable for both trace gas and O_4 dSCDs. Case studies results from Figs. 5 and S7, panels c) and d), indicate that the VMR retrieval quality decreases and exhibits a low bias when using a boundary layer zenith reference compared to reference spectra from higher altitudes. This observation is a direct result of SCD_{ref} being maximized for a boundary layer zenith spectrum and thus decreasing EA 0° dSCDs. Measured EA 0° dSCDs are further decreased for ΔSZA < 0°, where the

10   comparatively higher SZA of the reference spectrum increases SCD_{ref} even more. E.g. for SZA = 25°, ΔSZA = -15° and h_{ref} = 0.1 km (Figs. 5c and S7c), SCD_{ref} values averaged over aerosol profiles 1-3 are 3.8 x 10^{13} molec/cm^2 for the BrO a-profile, 7.6 x 10^{15} molec/cm^2 for the NO_2 a-profile, and 7.2 x 10^{12} molec/cm^2 for the IO a-profile, compared to 3.2 x 10^{13} molec/cm^2, 6.4 x 10^{15} molec/cm^2, and 6.1 x 10^{12} molec/cm^2 for SZA = 60°, ΔSZA = 35° and h_{ref} = 0.1 km (Figs. 5d and S7d) for BrO, NO_2, and IO,

15   respectively. For the optimized conditions, e.g. for SZA = 25°, ΔSZA = 0° and h_{ref} = 4.25 km (BrO, NO_2) or 14.75 km (IO) (Fig. 5a), SCD_{ref} values are 2.5 x 10^{13} molec/cm^2, 3.4 x 10^{15} molec/cm^2, and 3.9 x 10^{12} molec/cm^2 for BrO, NO_2 and IO, respectively. For VMR_{para} data that is not retrieved within error bounds, the ratio of EA 0° dSCDs over SCD_{ref} is typically smaller 2. These findings underline the importance of reference selection and minimizing SCD_{ref}.

20   Volkamer et al. 2015 compared ship-based and airborne MAX-DOAS during TORERO, under a case study where the trace gas profile above the ship was characterized by the aircraft. They found best agreement only when SCD_{ref} was accounted for in the ship MAX-DOAS retrievals; and show that the widely accepted assumption of SCD_{ref} = 0 can lead to bias of up to a factor of two for partial VCDs as retrieved from the ship (Volkamer et al., 2015). Maximizing knowledge about SCD_{ref} can also be

25   actively exploited to extend the information content in ground-based MAX-DOAS retrievals of free tropospheric BrO (Coburn et al., 2016).

Finding a suitable reference for O_4 measurements is less straightforward due to the multiple scattering effects described in Sect 4.1. In fact, using a high altitude zenith spectrum that minimizes SCD_{ref} here leads to a much stronger underestimation of extinction in the troposphere up to the point where extinction appears to be lower than that of a pure Rayleigh atmosphere. The key to a suitable O_4

5   reference is finding a reference for which Box-AMFs outside S are most similar to Box-AMFs outside S of the EA 0° spectrum, without minimizing the EA 0° dSCD too strongly. Based on our findings, EA 10° spectra from aircraft maximum altitude are a good match for these criteria, consistent with our earlier recommendation (Volkamer et al., 2015).

4.3.3 Optimized observing strategy parameterization retrieval

10   As discussed above, minimizing SCD_{ref} is the best strategy to minimize VMR_{para} errors. Aircraft measurements allow the recording of reference spectra at different geometries and altitudes, which renders AMAX-DOAS particularly suitable for the parameterization retrieval. For unknown trace gas and extinction profile shapes, it is advisable to record several references from different altitude and geometries to not limit the ability to actively minimize SCD_{ref}.

15   Data filters that work well for our sensitivity studies are 1) EA 0° dSCD limits of 1.5×10^{13} molec cm^{-2} for BrO, 2×10^{12} molec cm^{-2} for IO, and 2×10^{14} molec cm^{-2} for NO_2; 2) SZA limit of 60° for stratospheric absorbers; and 3) ΔSZA limit of -25° for $h_{ref} < 2$ km. Particularly for stratospheric absorbers VMR_{para} are on average retrieved more accurately for ΔSZA $>= 0°$. For a changing SZA and/or changing VCD_{strat}, the stratospheric correction benefits from continuous VCD characterization

20   by EA 10° measurements.

The interpolation parameter for O_4 dSCDs used in Eq. (5) need to be created for local conditions. In cases of strongly varying extinctions, interpolation might need to be replaced with a lookup table. For strong gradients in trace gas and/or aerosol extinction, optimal estimation retrieval is preferred.

5 Application to TORERO field data

During the TORERO field campaign BrO, IO, NO_2, CHOCHO, HCHO and O_4 were measured with the CU AMAX-DOAS instrument aboard the NSF/NCAR GV aircraft over the Eastern tropical Pacific Ocean. The TORERO field experiment took place in January/February, 2012. Seventeen research

5   flights were conducted over the tropical and sub-tropical Pacific, based out of Antofagasta, Chile and San Jose, Costa Rica. Further information on the campaign can be found in Volkamer et al. (2015). In this section, the parameterization retrieval is applied to TORERO field data. First select VMR_{para} profiles are compared with existing BrO, IO and NO_2 vertical profiles retrieved by optimal estimation (OE) inversion, followed by a discussion of retrieved BrO and IO VMRs for the whole campaign.

10   ### 5.1 AMAX-DOAS measurements and data analysis

The CU AMAX-DOAS instrument is described in detail elsewhere (Baidar et al., 2013b; Dix et al., 2013b; Volkamer et al., 2015). Briefly, the instrument consists of two synchronized spectrograph-detector units (Acton SP2150 / PIXIS400B CCD) that simultaneously observed the spectral ranges from 330-470 nm (0.7 nm Full Width Half Maximum (FWHM) optical resolution) to measure BrO, IO, NO_2,

15   and O_4 at 360 nm and from 440 – 700 nm (1.2 nm FWHM optical resolution) to observe O_4 at 477 nm. Telescopes to access forward, zenith and nadir viewing geometries are housed in a heated, wing-mounted pylon. The limb scanning telescope has a vertical dispersion of 0.17° and is actively angle stabilized to better 0.2° accuracy in real time. Most limb spectra were recorded with a time resolution of 30 s, which translates to a vertical resolution of 0.5 km or better for most ascents and descents of the

20   aircraft. BrO, IO, NO_2 and O_4 dSCDs were derived from scattered sun light spectra using the DOAS technique (Perner and Platt, 1979; Platt, 1994; Platt and Stutz, 2008) and the WinDOAS software package (Fayt and Van Roozendael, 2001). For further details, see Volkamer et al. (2015). The accuracy of our O_4 measurements has been assessed in a pure Rayleigh atmosphere (Spinei et al., 2015) and in the presence of aerosol (Volkamer et al., 2015). We found no need to apply a correction factor to the

25   measured O_4 (Wagner et al., 2009; Spinei et al., 2015; Volkamer et al., 2015).

BrO, IO and NO_2 dSCD data used for both the OE and the parameterization retrievals are quality filtered for instrument and data analysis effects as well as cloud filtered. The color ratio of the measured

intensities at 477 nm and 640 nm is used to identify clouds in the telescope's field of view and in close proximity. Once the color ratio falls below 2.1 for aircraft altitudes above 4 km and below 1.95 for aircraft altitudes below 4 km, dSCD data is filtered. The altitude distinction accounts for the color ratio also being affected by aerosol extinction, which is typically higher closer to the surface. Color ratio

5 thresholds are determined empirically and work well for most TORERO flights. To ensure that only cloudy dSCD data gets filtered, the color ratio filter is manually checked for each flight and changed if needed, based on flight video data. The profile case studies discussed in Section 5.3 are predominantly cloud free.

5.2 Optimal estimation profiles and parameterization retrieval

10 **Optimal estimation:** Concentration profiles for BrO, IO and NO_2 were retrieved from TORERO data by linear inversion of measured dSCDs using OE. The RTM McArtim was used to calculate weighting functions that serve as OE input. Radiation fields were constrained by in-situ pressure, temperature and water vapor measurements. CU AMAX-DOAS observations of O_4 at 360 and 477 nm were used to determine local aerosol extinction in a first step. Retrieved extinction profiles were then included in the

15 RTM to calculate weighting functions for the inversion. The number of independent concentration points is typically well aligned with the vertical resolution of the inversion. Control over radiative transfer has been demonstrated by comparison with in-situ and modelled H_2O data, with modelled NO_2, and comparison with aerosol extinction retrieved from high spectral resolution LIDAR (HSRL) and from Mie calculations based on aerosol size distributions measured by an in-situ ultra-high-sensitivity

20 aerosol spectrometer (UHSAS) (Volkamer et al., 2015).

Parameterization: The parameterized retrieval uses an almost identical RTM atmosphere, except that pressure, temperature and water vapor data are averaged over each full flight, instead of being averaged only over the profile time period. Reference spectra for both parameterization and OE dSCDs are identical, with one fixed reference per flight. Selection guidelines for references are discussed in

25 Volkamer et al. (2015). Since atmospheric conditions found in the TORERO study area are well represented in the sensitivity studies above, the same Box-AMFs and polynomial coefficients for the interpolation of measured O_4 dSCDs are used. Every research flight but one, RF08, provided

atmospheric conditions, where O_4 dSCD measurements from aircraft altitudes above 12 km could be considered Rayleigh measurements. Typically an upward angle scan covering EA 0°, 1°, 2°, 5° and 10° was used to absolutely scale measured O_4 dSCDs (see also Spinei et al., 2015). Atmospheric conditions that pass the above introduced cloud filter are instances where the aircraft flies high above low cloud

5   layers or vice versa. A series of preliminary sensitivity studies with cloud layers at different altitudes and trace gas profiles similar to the c-profiles here (Fig. 3), has shown that the ratio of measured and modelled O_4 dSCDs can serve as indicator for specific cloud situation. When flying above low cloud layers, VMR_{para} are typically retrieved within the established error bounds as long as the O_4 dSCD ratio stays below 1.15 at 360 nm and below 1.2 at 477 nm. For ratios between 1.15 and 1.3 at 360 nm and 1.2

10   and 1.4 at 477 nm, the measured O_4 dSCD is scaled to the equivalent of a 1.15 and 1.2 ratio respectively. Here, 5 percentage points are added to the error bound. Data points with higher O_4 ratios are filtered. When flying below a cloud cover, most data is retrieved within error bounds as long as the O_4 ratio is larger 0.5. Once it falls below 0.5 and the color ratio is larger 2.8, data is filtered out. All data points within 2 km of a solid cloud layer are filtered. HSRL data is used to get information on cloud

15   layer heights. Note that our cloud handling here is optimized for atmospheric conditions in the TORERO study area. Further sensitivity studies are warranted in other atmospheric settings, e.g. in instances where high aerosol extinction is present at higher altitudes.

Trace gas profile information above aircraft maximum altitude for BrO and NO_2 is taken from the Real-time Air Quality Modelling System (RAQMS) (Pierce et al., 2003, 2007). Corrections for dSCD

20   contributions from outside S are based on Eqs. (6) - (9) for NO_2 and IO. Stratospheric BrO VCDs are quantified by RAQMS, since the TORERO data set does not contain a sufficient amount of high signal to noise EA 10° spectra. For the TORERO BrO data set, maximum BrO $dSCD_{strat}$ (Eq. (8)) values are typically around $1-2 \times 10^{13}$ molec/cm^2 at SZA = 60°. Select comparison of stratospheric corrections retrieved from EA 10° measurements confirm the model based correction within an $2-3 \times 10^{13}$

25   molec/cm^2 uncertainty created by the EA 10° dSCD fit error. In order to calculate $AMF(t)_{refstrat}$ used in Eqs. (8) and (9), $AMF(t_0)_{refstrat}$ is scaled with the stratospheric geometric AMF, i.e., AMF = 1/COS(SZA), which saves further RTM computation time.

Layer n_{max}, which is the altitude that separates stratospheric and tropospheric corrections (see Sect. 2.2), is set to the maximum aircraft altitude for which the i=0 parameterization retrieval provides profile information. The layer n_{max} is identical to the maximum aircraft altitude of each individual flight, unless high altitude dSCD data has been filtered (clouds/quality assurance). Most TORERO flights targeted air

5   masses that are rather homogenous with respect to trace gas distributions. In order to calculate $dSCD^i_{trop}$ and $f_{TG}^{\ i}$ (Eqs. (3) and (7)), retrieved concentrations are averaged over the full flight, then interpolated and smoothed where needed, to minimize data scatter effects on the trace gas profile shape correction. During instances where the flight track crossed into stratospheric air, a second profile for BrO and NO_2 is created and used to calculate $dSCD^i_{trop}$ and $f_{TG}^{\ i}$ for these time periods. IO VMR data often showed

10   stronger variations below 5 km altitude within one flight. Here, up to three separate profiles per flight were created, while ensuring that profile dependent differences above 5 km in the final VMR_{para} do not exceed error bounds. For the direct profile comparison discussed in the following section, the calculation of $dSCD^i_{trop}$ and $f_{TG}^{\ i}$ is based on results from the profile time period only. The errors reported for the parameterized data are those discussed above and in Section 4.3.

15 **5.3 Comparison of optimal estimation and parameterization profiles**

Figure 7 shows a comparison of VMR data retrieved by OE and by the parameterization method for select profiles of BrO, IO and NO_2 from the TORERO campaign for flights RF01, RF12 and RF17 (Volkamer et al., 2015; Wang et al., 2015). Parameterized VMRs are reported at aircraft altitude, i.e. the altitude for which the Box-AMFs are calculated. Even though all applied equations are based on a

20   discrete altitude grid that assumes a constant concentration within the altitude layer n, the spread seen within the same grid layer could be a reflection of a true trace gas gradient. Here the parameterization retrieval can provide additional information that is lost to the smoothing error of the OE method. The pronounced IO layer in the RF01 profile presents a good example of this effect. The VMR_{para} data points between 1.9 and 2.4 km clearly outline the IO peak at 2.25 km, whereas the OE data reports

25   discrete values for 1.75, 2.25 and 2.75 km. Note that the lines connecting the OE data points in Fig. 7 are only plotted to help guide the eye along the profile shape. All data points overlap within error bars, but the parameterization reveals steeper IO gradients indicative of less smoothing. In order to calculate

correlations, the VMR_{OE} data is interpolated to the VMR_{para} data. Results for all three trace gases are shown in Fig. 8. To increase statistics for the correlation, trace gas profiles from more flights are included, i.e. RF01, RF04, RF05, RF12, RF14 and RF17 for BrO and IO and RF12 and RF17 for NO_2 as reported in Wang et al. (2015) and Volkamer et al. (2015). A least orthogonal distance fit is applied

5   to consider the x- and y-error. Offset and slopes are reported for a 95 % confidence interval and included in the individual trace gas panels. Also here the agreement between VMR_{para} and VMR_{OE} is excellent. Offset values are insignificant, while slopes of 0.95 ±0.14 for BrO, 1.00 ±0.12 for IO, and 0.90 ±0.51 for NO_2 are within expectation based on the sensitivity studies (see Sect. 4.3). The comparatively large error for the NO_2 slope coefficient is driven by large relative x- and y-errors and

10   caused by NO_2 VMRs close to the 10 pptv detection limit. The actual correlation of the data points shown in Fig. 8 is much tighter than what error bars allow.

5.4 TORERO BrO and IO VMR_{para} results

Figure 9 shows BrO and IO VMR_{para} results for all 17 TORERO RFs (but RF08). Altitudes of retrieved VMR data are plotted over latitude and are color coded by mixing ratios. BrO is consistently low in the

15   boundary layer and almost never exceeds the detection limit of 0.5 pptv. Particularly in the tropical free troposphere Fig. 9 shows a significant variability for BrO. VMRs larger 1 pptv at altitudes above 8 km are also found in air without significant stratospheric influence and remain currently unexplained. (Wang et al., 2015).

As expected, IO shows maxima in the boundary layer, but also a prevalent distribution throughout the

20   troposphere. Our data suggest the existence of a hemispheric gradient with higher IO in the southern hemisphere. The observed halogen abundance over the tropical Eastern Pacific is not yet fully understood and has implications for ozone depletion, atmospheric oxidation capacity and mercury oxidation (Wang et al., 2015). The TORERO BrO and IO results show that the parametrization retrieval of VMRs along complete flight tracks enables a summary view of AMAX-DOAS results, which allows

25   an assessment on the consistency of data variability or gradients across the whole study area.

6 Conclusions and Outlook

The parameterization retrieval is a robust tool to convert AMAX-DOAS EA0° dSCDs of BrO, IO and NO$_2$ directly into VMRs. Flight tracks that vary altitude frequently provide the best results, because the iterative approach increases the accuracy of VMR$_{para}$ by utilizing profile information gained from ascent

5 or descent measurements. The magnitude of the stratospheric correction is constrained from measurements of EA 10° dSCD at high altitude. Based on our sensitivity studies on simulated data and application to field data, we conclude:

- The method is applicable over a wide range of atmospheric conditions and measurement geometries. VMRs of trace gases with significant stratospheric contributions to the VCDs can be retrieved for SZAs

10 0° to 60°, and for tropospheric trace gases for SZAs 0° to 70°, the latter being the full range covered by our sensitivity studies. VMR$_{para}$ data are on average within 10 - 15 % of VMR$_{true}$. Errors that arise from suboptimal reference spectra are either accounted for by the dSCD$_c^i$ correction or are avoided by applying filters. Actively minimizing SCD$_{ref}$ based on reference selection improves the accuracy of the parameterization retrieval.

15 - The comparison of VMR$_{para}$ field data with VMR$_{OE}$ shows excellent agreement within the error bounds established by the sensitivity studies. Correlations of 10 % and better are within expectations, and further corroborate that the parameterization retrieval is suitable for the analysis of field data.

- Using O$_4$ dSCDs as scaling factor for aerosol extinction is a viable tool for altitude ranges between 0 and 15 km, but not at higher altitudes, where O$_4$ contributions from outside S are a significant fraction

20 of the measured O$_4$ dSCDs and become difficult to account for.

- The retrieval is straightforward for gases that do not have a significant presence in the stratosphere. For gases with a significant presence in the stratosphere, the error can be reduced by following the recommendations given in Sect. 4.3.3.

- The retrieval has a duty cycle of 44.3 % and 60.1 %, for BrO and IO VMR$_{para}$, based on the number of

25 available EA 0° spectra. Data quality, parameterization method and cloud filters are responsible for the removal of 23.7 %, 10.2 %, and 21.8 % of the BrO data, respectively; and 10.5 %, 3.2 %, and 26.2 %

for IO data, respectively. The method filter is the smallest contribution for both trace gases, which underlines the statistical advantage of the parametrization method over OE.

For future use, the method can easily be adapted for the retrieval of other absorbers like glyoxal, formaldehyde or HONO. The inherently fast conversion of dSCDs into VMRs can also serve as a tool

5   for near real-time VMR retrievals in the field. Future work will include optimizing the parameterization retrieval for 1) polluted environments, i.e. atmospheres with high NO_2 and/or aerosol extinction; 2) for SZA conditions outside current filters, and 3) minimizing the need for cloud-filtering.

Acknowledgements

10   The TORERO project was funded by the National Science Foundation under award AGS-1104104 (PI: R. Volkamer). The involvement of the NSF-sponsored Lower Atmospheric Observing Facilities, managed and operated by the National Center for Atmospheric Research (NCAR) Earth Observing Laboratory (EOL), is acknowledged. R. Volkamer acknowledges financial support from National Science Foundation Faculty Early Career Development (CAREER) award ATM-0847793, Department

15   of Energy award DE-SC0006080 and Electric Power Research Institute (EPRI) contracts EP-P27450/C13049 and EP-P32238/C14974 that supported the development of the AMAX-DOAS instrument and software/data analysis tools used in this study. We thank S. Baidar for support on data analysis.

Table 1 RTM settings

Parameter	RTM Value
Wavelength	350 nm (BrO); 428 nm (IO); 447 nm (NO_2); 360 and 477 nm (O_4)
SZA	0°, 10°, 25°, 40°, 50°, 60°, 70°
SRAA	90°
EA	0°, 10°, 90°
Altitude	EA0°: 0.1 km, 0.25 - 14.75 km in 0.5 km increments EA 10°: 11.25 km, 12.25 km, 13.25 km 14.25 km, 14.75 km EA90°: 0.1 km, 4.25 km, 7.75 km, 11.25 km, 12.25 km
ground albedo	350/360 nm: 0.05, 428-477 nm: 0.08
g-parameter[1]	marine: 0.75; urban: 0.69; mixed: 0.72
SSA[1]	marine: 0.98; urban: 350/ 360 nm; 0.92, 428-477 nm: 0.94; mixed: 0.96

[1] Settings based on Dubovic et al. (2002)

Table 2 VMR retrieval results for synthetic data

Trace Gas	atmosphere	Mean	Standard Deviation	Within error[1] [%]	Within DL[2] [%]
BrO	Rayleigh	0.99	0.06	100	100
BrO	Aerosol 1	1.00	0.11	99.9	99.9
BrO	Aerosol 2	1.01	0.14	99.3	97.8
BrO	Aerosol 3	1.04	0.15	99.7	99.6
IO	Rayleigh	0.97	0.05	100	99.4
IO	Aerosol 1	0.92	0.07	98.8	90.8
IO	Aerosol 2	0.88	0.09	92.8	83.8
IO	Aerosol 3	0.90	0.13	91.9	85.0
NO_2	Rayleigh	0.99	0.07	99.5	96.7
NO_2	Aerosol 1	1.00	0.09	98.7	87.9
NO_2	Aerosol 2	1.00	0.14	94.9	85.3
NO_2	Aerosol 3	1.02	0.14	95.8	78.7

[1] ±0.5 pptv or 30 % for BrO, ±0.05 pptv or 20 % for IO, ±10 pptv or 30 % for NO_2

[2] ±0.5 pptv for BrO, ±0.05 pptv for IO, ±10 pptv for NO_2
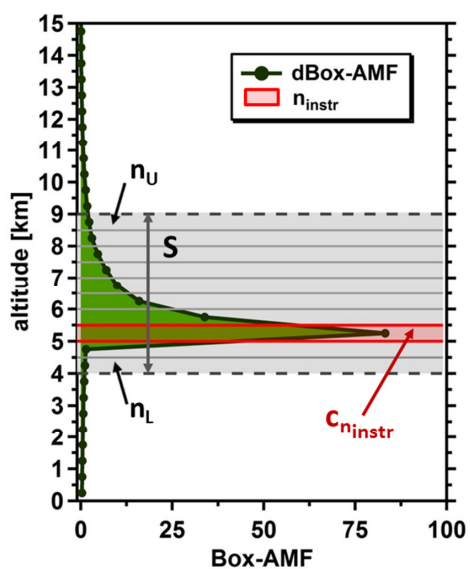
Figure 1. dBox-AMF values modeled at 477 nm on a 0.5 km grid (grey lines within S) for an EA 0° dSCD measurement at 5.25 km and a zenith reference from 7.75 km. Grey shading indicates the sensitive range S demarked by the lower and upper limit layers n_L and n_U. Green shading emphasizes the strong sensitivity of the EA 0° measurement at instrument altitude, while the red box marks the instrument layer n_{instr} for which the trace gas concentration $c_{n_{instr}}$ is being retrieved.
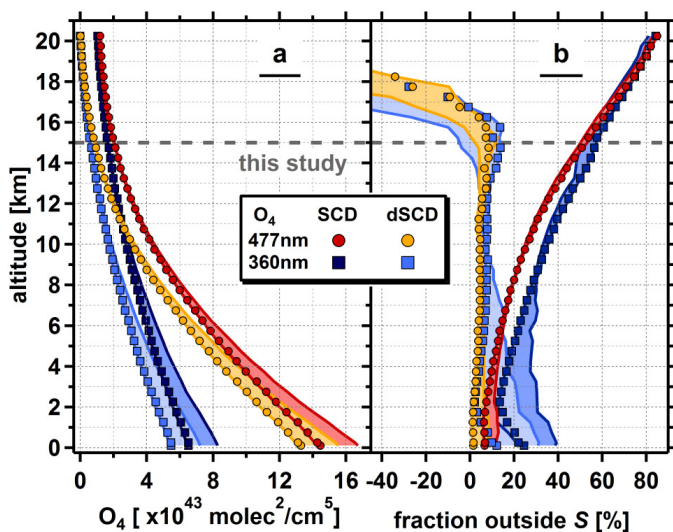
Figure 2. Sensitivity of EA0° O_4 measurements at 360 and 477 nm with SZA = 25° (markers) and SZA = 0° - 70° (shadings). (a) O_4 SCD and dSCDs values. The reference spectrum to create dSCDs is an EA 10° spectrum from 14.25 km with SZA = 25°. (b) Fraction of the total SCD/dSCD coming from outside the sensitive range S.
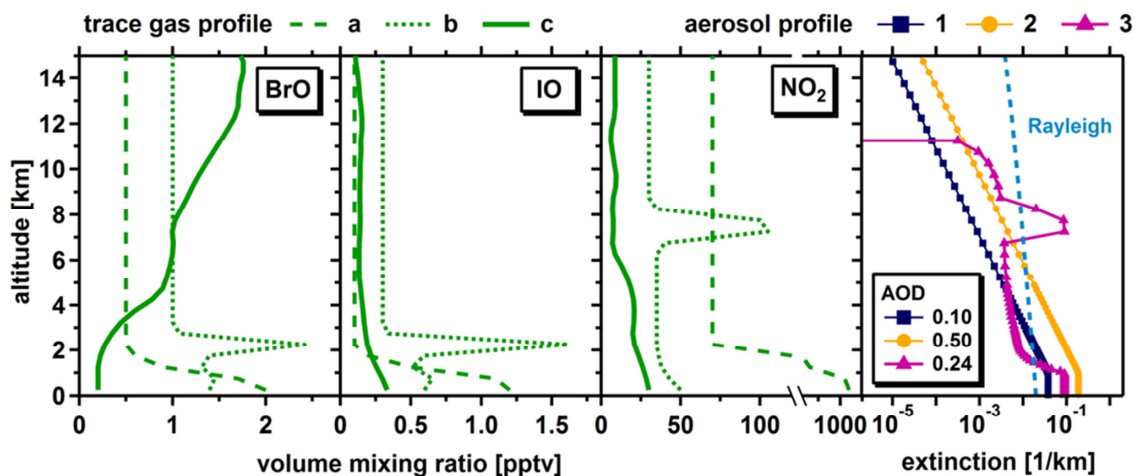
Figure 3. Trace gas volume mixing ratio and aerosol extinction profiles used to simulate dSCD data for sensitivity studies.
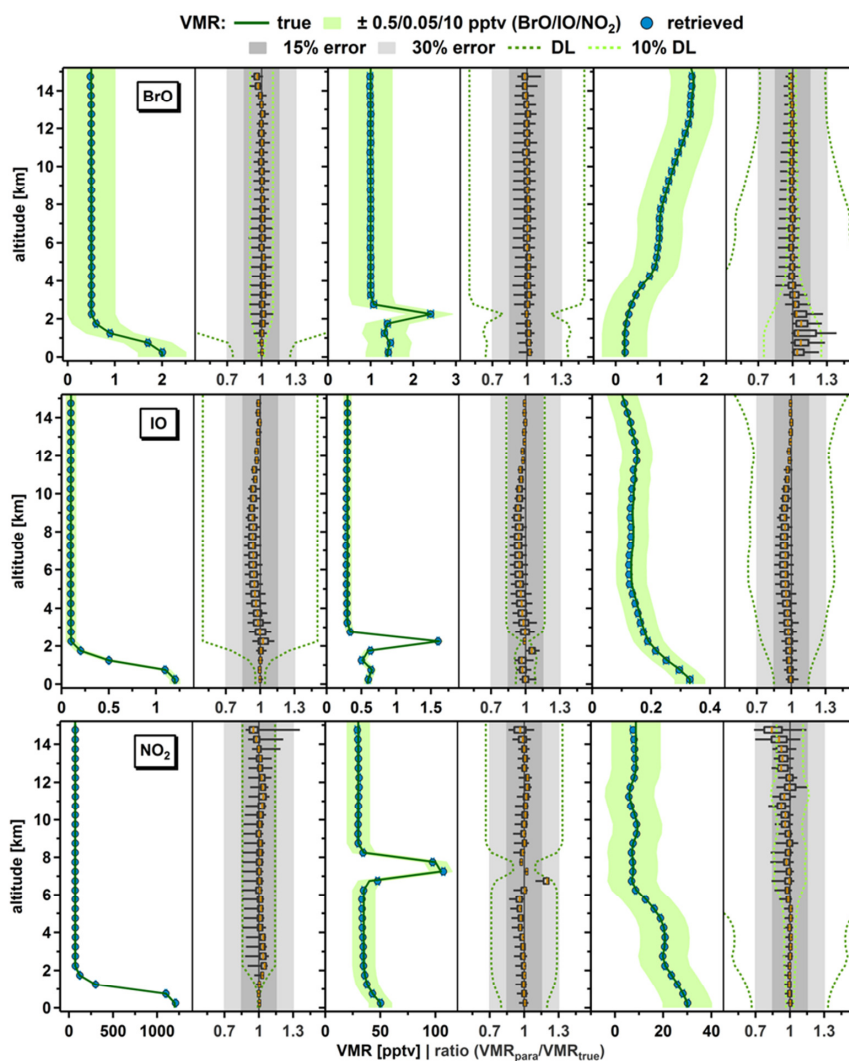
Figure 4. Retrieved VMR for BrO (top), IO (middle) and NO_2 (bottom) a-, b-, and c-profiles (left to right) using dSCD data simulated for a Rayleigh atmosphere. Individual left panels show VMR_{para} average and standard deviation. Original trace gas profiles are included as reference and green shading denotes individual trace gas VMR error bounds. Right panels display altitude resolved whisker plots of the ratios of VMR_{para} over VMR_{true}, showing the mean (orange) and 5, 25, 75 and 95 percentiles. Grey shaded areas indicate 15 % and 30 % error; green dashed lines show trace gas detection limits.
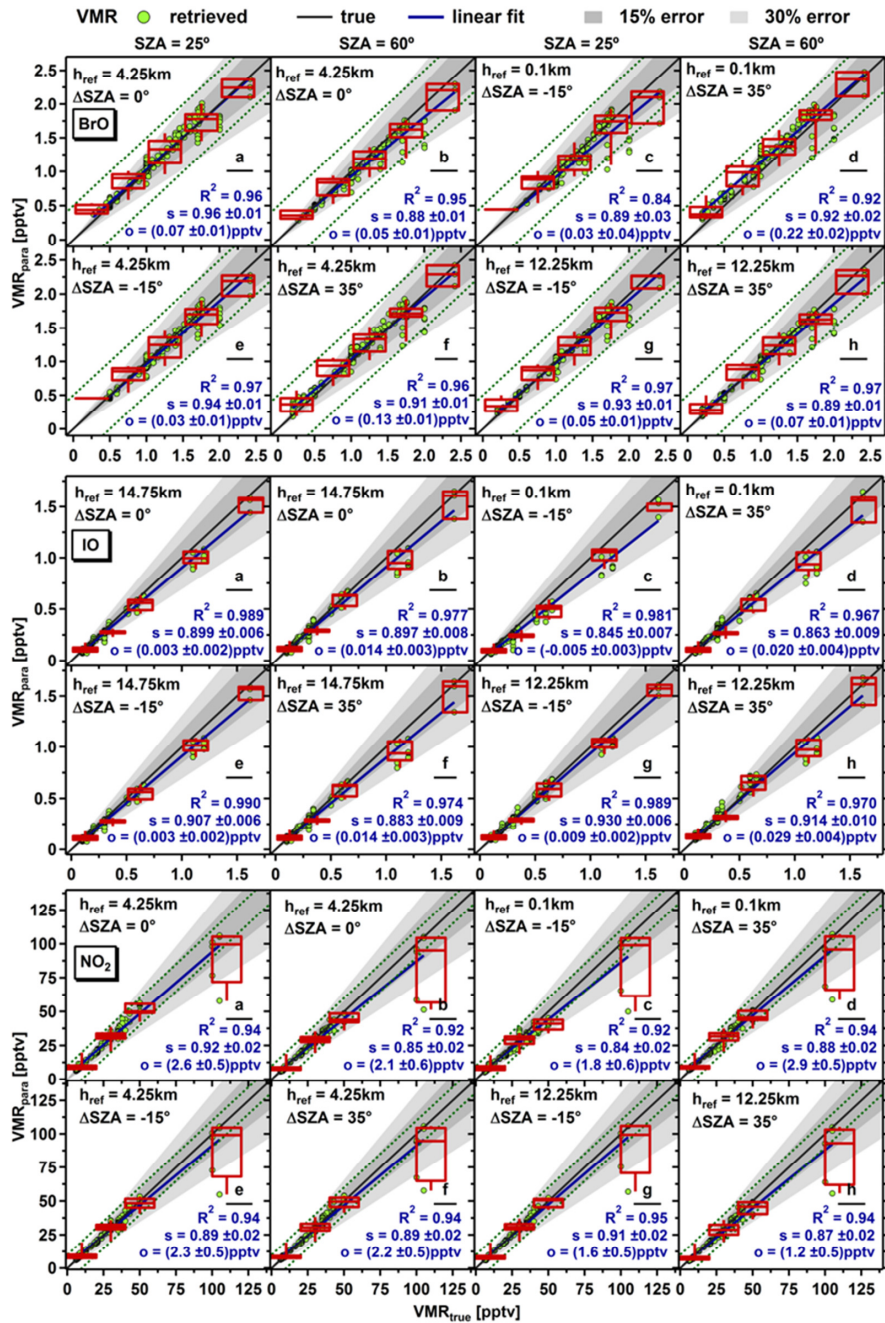
Figure 5. VMR_{para} over VMR_{true} for BrO (top), IO (middle) and NO_2 (bottom) averaged over all BrO and IO trace gas, over NO_2 b- and c-profiles and over all aerosol profiles for select SZA, ΔSZA and h_{ref}. The panel columns alternate between low (SZA = 25°) and high SZA (SZA = 60°). The whisker plots show 5, 25, 75 and 95 percentiles for binned VMR_{para} data. Grey shaded areas indicate 15 % and 30 % error. Linear fits and fit parameter (s: slope, o: offset) are included in each panel.
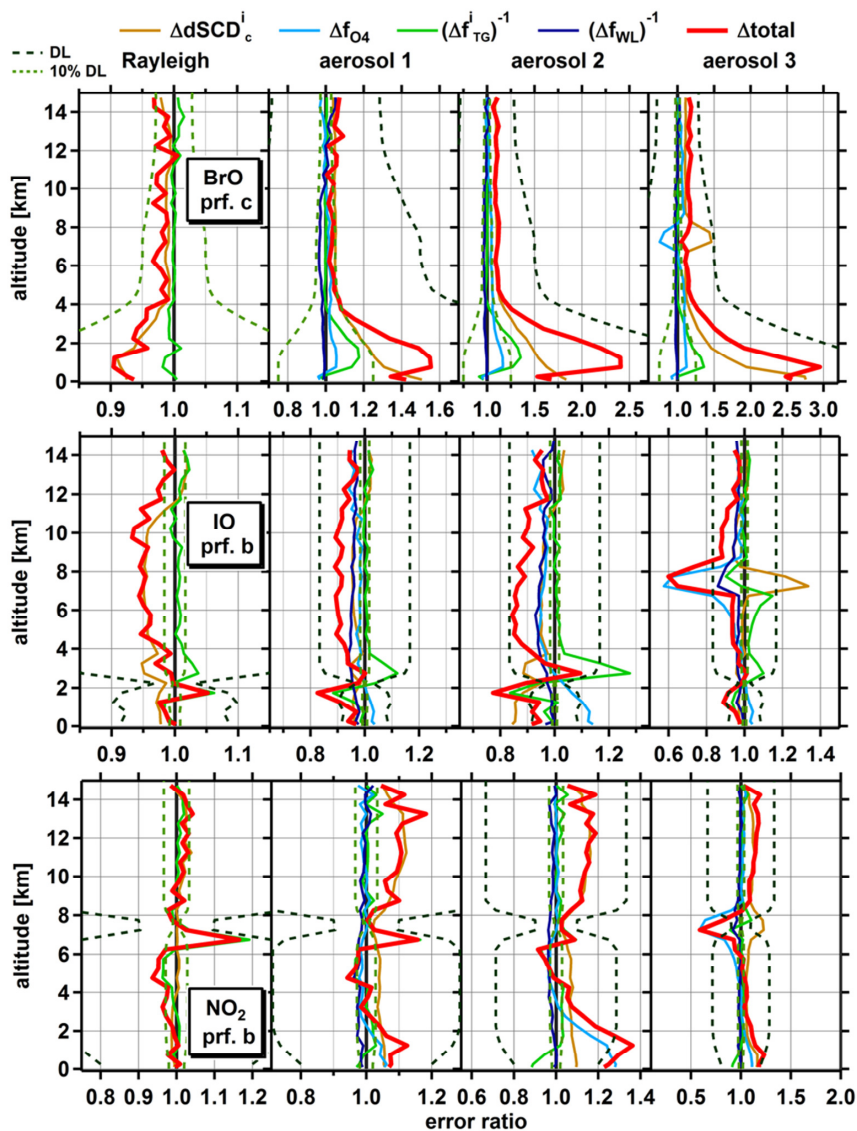
Figure 6. Total error, Δtotal, and error ratios of individual components of Eq. (1) for BrO c-profile (top), IO b-profile (middle), and NO_2 b-profile (bottom) for Rayleigh and aerosol case studies with SZA = 25° and ΔSZA = 25°. Reference altitude for BrO and NO_2 is 4.25 km and 14.75 km for IO. Green dashed lines show trace gas detection limits. Note the different x-axis scaling for individual panels.
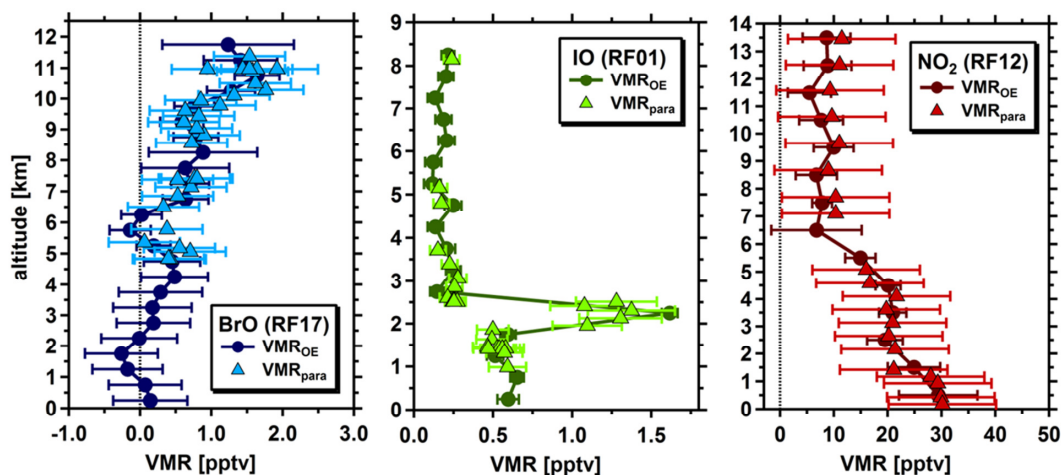
Figure 7. Comparison of VMR data retrieved from TORERO AMAX-DOAS data using the parameterization retrieval or optimal estimation (OE) for select BrO (left), IO (middle), and NO_2 (right) profiles.
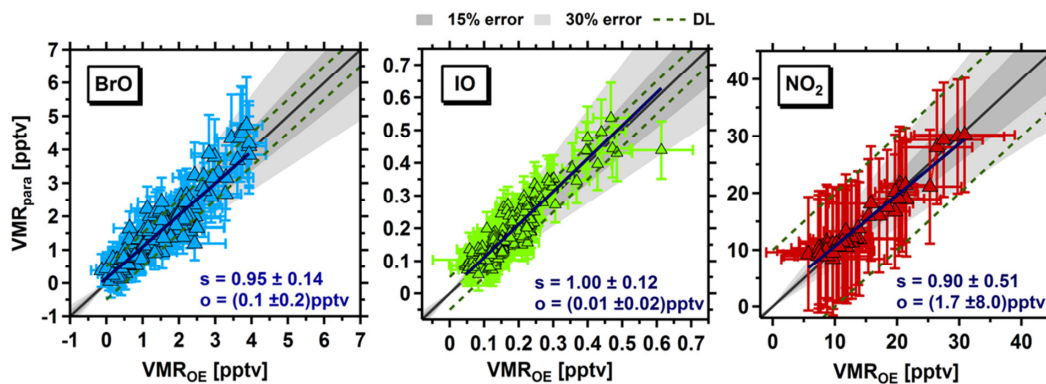
5 **Figure 8.** Correlations of TORERO AMAX-DOAS VMR data retrieved by parameterization (param.) and optimal estimation (OE) for BrO (left), IO (middle), and NO_2 (right). Grey shaded areas indicate 15 % and 30 % error; green dashed lines show trace gas detection limits. Linear fits and fit parameter (s: slope, o: offset) are included in each panel.
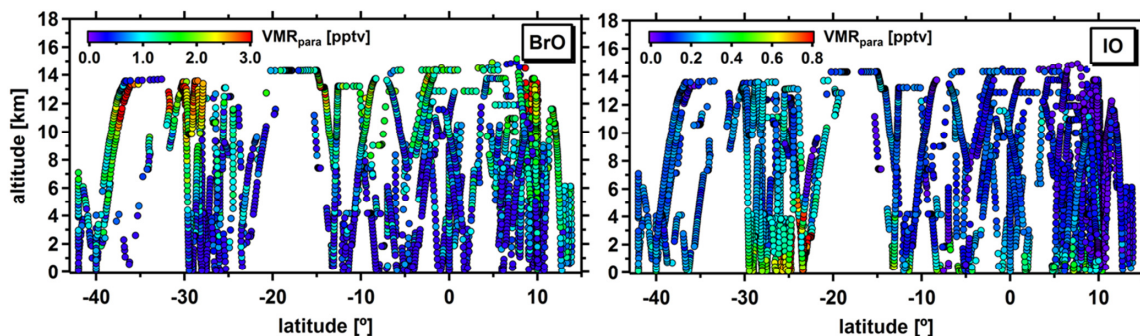
Figure 9. TORERO AMAX-DOAS BrO (left) and IO (right) VMR$_{para}$ data for the complete campaign. Plotted are aircraft altitudes over latitude, color coded by VMR$_{para}$. Longitudes covered are 70° W to 105° W.

5 **References:**

Baidar, S., Volkamer, R., Alvarez, R., Brewer, A., Davies, F., Langford, A., Oetjen, H., Pearson, G., Senff, C. and Hardesty, R. M.: Combining Active and Passive Airborne Remote Sensing to Quantify NO2 and Ox Production near Bakersfield, CA, Br. J. Environ. Clim. Chang., 3, 566–586, doi:10.9734/BJECC/2013/5740, 2013a.

10 Baidar, S., Oetjen, H., Coburn, S., Dix, B., Ortega, I., Sinreich, R. and Volkamer, R.: The CU Airborne MAX-DOAS instrument: vertical profiling of aerosol extinction and trace gases, Atmos. Meas. Tech., 6, 719–739, doi:10.5194/amt-6-719-2013, 2013b.

Baidar, S., Hardesty, R. M., Kim, S.-W., Langford, A. O., Oetjen, H., Senff, C., Trainer, M. and Volkamer, R.: Weakening of the Weekend Ozone Effect over California's South Coast Air Basin,
15 Geophys. Res. Lett., doi:10.1002/2015GL066419, 2015.

Bruns, M., Buehler, S. A., Burrows, J. P., Richter, A., Rozanov, A., Wang, P., Heue, K. P., Platt, U., Pundt, I. and Wagner, T.: NO2 profile retrieval using airborne multi axis UV-visible skylight absorption measurements over central Europe, Atmos. Chem. Phys., 6, 3049–3058, 2006.

Coburn, S., Dix, B., Edgerton, E., Holmes, C. D., Kinnison, D., Liang, Q., ter Schure, A., Wang, S. and

Volkamer, R.: Mercury oxidation from bromine chemistry in the free troposphere over the southeastern US, Atmos. Chem. Phys., 16, 3743–3760, doi:10.5194/acp-16-3743-2016, 2016.

Coburn, S. C., Dix, B. K., Sinreich, R., Terschure, A. F., Edgerton, E. S. and Volkamer, R.: Measurements of halogen oxides and speciated mercury at a coastal site in Pensacola, FL, Geochim.
5   Cosmochim.   Acta,   74,   A184–A184   [online]   Available   from: http://apps.webofknowledge.com/full_record.do?product=UA&search_mode=GeneralSearch&qid=1&SID=2Ep7T6Y6Z47pcpRD1U4&excludeEventConfig=ExcludeIfFromFullRecPage&page=3&doc=33 (Accessed 30 October 2015), 2010.

Deutschmann, T., Beirle, S., Frieß, U., Grzegorski, M., Kern, C., Kritten, L., Platt, U., Prados-Román,
10   C., Puķīte, J., Wagner, T., Werner, B. and Pfeilsticker, K.: The Monte Carlo atmospheric radiative transfer model McArtim: Introduction and validation of Jacobians and 3D features, J. Quant. Spectrosc. Radiat. Transf., 112, 1119–1137, doi:10.1016/j.jqsrt.2010.12.009, 2011.

Dix, B., Brenninkmeijer, C. A. M., Friess, U., Wagner, T. and Platt, U.: Airborne multi-axis DOAS measurements of atmospheric trace gases on CARIBIC long-distance flights, Atmos. Meas. Tech., 2,
15   639–652, 2009.

Dix, B., Baidar, S., Bresch, J. F., Hall, S. R., Schmidt, K. S., Wang, S. and Volkamer, R.: Detection of iodine monoxide in the tropical free troposphere., Proc. Natl. Acad. Sci. U. S. A., 110, 2035–40, doi:10.1073/pnas.1212386110, 2013.

Dubovik, O., Holben, B., Eck, T., Smirnov, A., Kaufman, Y., King, M., Tanre, D. and Slutsker, I.:
20   Variability of absorption and optical properties of key aerosol types observed in worldwide locations, J. Atmos. Sci., 59, 590–608, doi:10.1175/1520-0469(2002)0592.0.CO;2, 2002.

Fayt, C. and Van Roozendael, M.: WinDOAS 2.1–Software user manual, 2001.

Henyey, L. C. and Greenstein, J. L.: Diffuse radiation in the Galaxy, Astrophys. J., 93, 70, doi:10.1086/144246, 1941.

25   Heue, K., Richter, A., Bruns, M., Burrows, J., von Friedeburg, C., Platt, U., Pundt, I., Wang, P. and Wagner, T.: Validation of SCIAMACHY tropospheric NO2-columns with AMAXDOAS

measurements, Atmos. Chem. Phys., 5, 1039–1051, 2005.

Heue, K.-P., Brenninkmeijer, C. A. M., Baker, A. K., Rauthe-Schöch, A., Walter, D., Wagner, T., Hörmann, C., Sihler, H., Dix, B., Frieß, U., Platt, U., Martinsson, B. G., van Velthoven, P. F. J., Zahn, A. and Ebinghaus, R.: SO_2 and BrO observation in the plume of the Eyjafjallajökull volcano 2010:
5 CARIBIC and GOME-2 retrievals, Atmos. Chem. Phys., 11, 2973–2989, doi:10.5194/acp-11-2973-2011, 2011.

Heue, K.-P., Riede, H., Walter, D., Brenninkmeijer, C. A. M., Wagner, T., Frieß, U., Platt, U., Zahn, A., Stratmann, G. and Ziereis, H.: CARIBIC DOAS observations of nitrous acid and formaldehyde in a large convective cloud, Atmos. Chem. Phys., 14, 6621–6642, doi:10.5194/acp-14-6621-2014, 2014.

10 Hönninger, G., von Friedeburg, C. and Platt, U.: Multi axis differential optical absorption spectroscopy (MAX-DOAS), Atmos. Chem. Phys., 4, 231–254, 2004.

Irie, H., Takashima, H., Kanaya, Y., Boersma, K. F., Gast, L., Wittrock, F., Brunner, D., Zhou, Y. and Van Roozendael, M.: Eight-component retrievals from ground-based MAX-DOAS observations, Atmos. Meas. Tech., 4, 1027–1044, doi:10.5194/amt-4-1027-2011, 2011.

15 Melamed, M. L., Solomon, S., Daniel, J. S., Langford, A. O., Portmann, R. W., Ryerson, T. B., Nicks, Jr., D. K. and McKeen, S. A.: Measuring reactive nitrogen emissions from point sources using visible spectroscopy from aircraft, J. Environ. Monit., 5, 29–34, doi:10.1039/b204220g, 2003.

Merlaud, A., Van Roozendael, M., Theys, N., Fayt, C., Hermans, C., Quennehen, B., Schwarzenboeck, A., Ancellet, G., Pommier, M., Pelon, J., Burkhart, J., Stohl, A. and De Mazière, M.: Airborne DOAS
20 measurements in Arctic: vertical distributions of aerosol extinction coefficient and NO_2 concentration, Atmos. Chem. Phys., 11, 9219–9236, doi:10.5194/acp-11-9219-2011, 2011.

Oetjen, H., Baidar, S., Krotkov, N. A., Lamsal, L. N., Lechner, M. and Volkamer, R.: Airborne MAX-DOAS measurements over California: Testing the NASA OMI tropospheric NO 2 product, J. Geophys. Res. Atmos., 118, 7400–7413, doi:10.1002/jgrd.50550, 2013.

25 Perner, D. and Platt, U.: Detection of nitrous acid in the atmosphere by differential optical absorption, Geophys. Res. Lett., 6, 917–920, doi:10.1029/GL006i012p00917, 1979.

Pierce, R. B., Al-Saadi, J. A., Schaack, T., Lenzen, A., Zapotocny, T., Johnson, D., Kittaka, C., Buker, M., Hitchman, M. H., Tripoli, G., Fairlie, T. D., Olson, J. R., Natarajan, M., Crawford, J., Fishman, J., Avery, M., Browell, E. V., Creilson, J., Kondo, Y. and Sandholm, S. T.: Regional Air Quality Modeling System (RAQMS) predictions of the tropospheric ozone budget over east Asia, J. Geophys. Res. Atmos., 108, doi:10.1029/2002JD003176, 2003.

Pierce, R. B., Schaack, T., Al-Saadi, J. A., Fairlie, T. D., Kittaka, C., Lingenfelser, G., Natarajan, M., Olson, J., Soja, A., Zapotocny, T., Lenzen, A., Stobie, J., Johnson, D., Avery, M. A., Sachse, G. W., Thompson, A., Cohen, R., Dibb, J. E., Crawford, J., Rault, D., Martin, R., Szykman, J. and Fishman, J.: Chemical data assimilation estimates of continental U.S. ozone and nitrogen budgets during the Intercontinental Chemical Transport Experiment–North America, J. Geophys. Res., 112, D12S21, doi:10.1029/2006JD007722, 2007.

Platt, U.: Differential Optical Absorption Spectroscopy (DOAS), in Chemical Analysis Series 127: Air monitoring by spectroscopic techniques, edited by M. W. Sigrist, pp. 27–84, John Wiley & Sons, Inc., New York., 1994.

Platt, U. and Stutz, J.: Differential Optical Absorption Spectroscopy, Springer, Heidelberg., 2008.

Prados-Roman, C., Butz, A., Deutschmann, T., Dorf, M., Kritten, L., Minikin, A., Platt, U., Schlager, H., Sihler, H., Theys, N., Van Roozendael, M., Wagner, T. and Pfeilsticker, K.: Airborne DOAS limb measurements of tropospheric trace gas profiles: case studies on the profile retrieval of O_4 and BrO, Atmos. Meas. Tech., 4, 1241–1260, doi:10.5194/amt-4-1241-2011, 2011.

Schreier, S. F., Richter, A., Wittrock, F. and Burrows, J. P.: Estimates of free-tropospheric NO2 and HCHO mixing ratios derived from high-altitude mountain MAX-DOAS observations at midlatitudes and in the tropics, Atmos. Chem. Phys., 16, 2803–2817, 2016.

Sinreich, R., Coburn, S., Dix, B. and Volkamer, R.: Ship-based detection of glyoxal over the remote tropical Pacific Ocean, Atmos. Chem. Phys., 10, 11359–11371, doi:10.5194/acp-10-11359-2010, 2010.

Sinreich, R., Merten, A., Molina, L. and Volkamer, R.: Parameterizing radiative transfer to convert MAX-DOAS dSCDs into near-surface box-averaged mixing ratios, Atmos. Meas. Tech., 6, 1521–1532,

doi:10.5194/amt-6-1521-2013, 2013.

Spinei, E., Cede, A., Herman, J., Mount, G. H., Eloranta, E., Morley, B., Baidar, S., Dix, B., Ortega, I., Koenig, T. and Volkamer, R.: Ground-based direct-sun DOAS and airborne MAX-DOAS measurements of the collision-induced oxygen complex, O_2O_2, absorption with significant pressure and temperature differences, Atmos. Meas. Tech., 8, 793–809, doi:10.5194/amt-8-793-2015, 2015.

Thalman, R. and Volkamer, R.: Temperature dependent absorption cross-sections of O2-O2 collision pairs between 340 and 630 nm and at atmospherically relevant pressure., Phys. Chem. Chem. Phys., 15, 15371–81, doi:10.1039/c3cp50968k, 2013.

Volkamer, R., Baidar, S., Campos, T. L., Coburn, S., DiGangi, J. P., Dix, B., Eloranta, E. W., Koenig, T. K., Morley, B., Ortega, I., Pierce, B. R., Reeves, M., Sinreich, R., Wang, S., Zondlo, M. A. and Romashkin, P. A.: Aircraft measurements of BrO, IO, glyoxal, NO2, H2O, O2–O2 and aerosol extinction profiles in the tropics: comparison with aircraft-/ship-based in situ and lidar measurements, Atmos. Meas. Tech., 8, 2121–2148, doi:10.5194/amt-8-2121-2015, 2015.

Wagner, T., Dix, B., Friedeburg, C. v., Frieß, U., Sanghavi, S., Sinreich, R. and Platt, U.: MAX-DOAS O4 measurements: A new technique to derive information on atmospheric aerosols-Principles and information content, J. Geophys. Res. Atmos., 109, doi:10.1029/2004JD004904, 2004.

Wagner, T., Deutschmann, T. and Platt, U.: Determination of aerosol properties from MAX-DOAS observations of the Ring effect, Atmos. Meas. Tech., 2, 495–512, 2009.

Wang, P., Richter, A., Bruns, M., Rozanov, V., Burrows, J., Heue, K., Wagner, T., Pundt, I. and Platt, U.: Measurements of tropospheric NO2 with an airborne multi-axis DOAS instrument, Atmos. Chem. Phys., 5, 337–343, 2005.

Wang, P., Richter, A., Bruns, M., Burrows, J., Scheele, R., Junkermann, W., Heue, K., Wagner, T., Platt, U. and Pundt, I.: Airborne multi-axis DOAS measurements of tropospheric SO2 plumes in the Po-valley, Italy, Atmos. Chem. Phys., 6, 329–338, 2006.

Wang, S., Schmidt, J. A., Baidar, S., Coburn, S., Dix, B., Koenig, T. K., Apel, E., Bowdalo, D., Campos, T. L., Eloranta, E., Evans, M. J., DiGangi, J. P., Zondlo, M. A., Gao, R.-S., Haggerty, J. A.,

Hall, S. R., Hornbrook, R. S., Jacob, D., Morley, B., Pierce, B., Reeves, M., Romashkin, P., Ter Schure, A. and Volkamer, R.: Active and widespread halogen chemistry in the tropical and subtropical free troposphere., Proc. Natl. Acad. Sci. U. S. A., 112, 9281–6, doi:10.1073/pnas.1505142112, 2015.